JAEA-Data/Code
2016-014
DOI:10.11484/jaea-data-code-2016-014

A Terrestrial Ecosystem Model (SOLVEG) Coupled with Atmospheric Gas and Aerosol Exchange Processes

Genki KATATA and Masakazu OTA

Environment and Radiation Sciences Division
Nuclear Science and Engineering Center
Sector of Nuclear Science Research

January 2017

Japan Atomic Energy Agency

日本原子力研究開発機構

JAEA-Data/Code

本レポートは国立研究開発法人日本原子力研究開発機構が不定期に発行する成果報告書です。
本レポートの入手並びに著作権利用に関するお問い合わせは、下記あてにお問い合わせ下さい。
なお、本レポートの全文は日本原子力研究開発機構ホームページ（http://www.jaea.go.jp）
より発信されています。

国立研究開発法人日本原子力研究開発機構 研究連携成果展開部 研究成果管理課
〒319-1195 茨城県那珂郡東海村大字白方 2 番地4
電話 029-282-6387, Fax 029-282-5920, E-mail:ird-support@jaea.go.jp

This report is issued irregularly by Japan Atomic Energy Agency.
Inquiries about availability and/or copyright of this report should be addressed to
Institutional Repository Section,
Intellectual Resources Management and R&D Collaboration Department,
Japan Atomic Energy Agency.
2-4 Shirakata, Tokai-mura, Naka-gun, Ibaraki-ken 319-1195 Japan
Tel +81-29-282-6387, Fax +81-29-282-5920, E-mail:ird-support@jaea.go.jp

JAEA-Data/Code 2016-014

A Terrestrial Ecosystem Model (SOLVEG) Coupled with Atmospheric Gas and Aerosol Exchange Processes

Genki KATATA and Masakazu OTA

Environment and Radiation Sciences Division
Nuclear Science and Engineering Center
Sector of Nuclear Science Research
Japan Atomic Energy Agency
Tokai-mura, Naka-gun, Ibaraki-ken

(Received November 10, 2016)

In order to predict the impact of atmospheric pollutants (gases and aerosols) to the terrestrial ecosystem, new schemes for calculating the processes of dry deposition of gases and aerosols, and water and carbon cycles in terrestrial ecosystems were implemented in the one-dimensional atmosphere-SOiL-VEGetation model, SOLVEG. We made performance tests at various vegetation areas to validate the newly developed schemes. In this report, the detail in each modeled process is described with an instruction how to use the modified SOLVEG. The framework of “terrestrial ecosystem model” was developed for investigation of a change in water, energy, and carbon cycles associated with global warming and air pollution and its impact on terrestrial ecosystems.

Keywords: Land Surface Model, Atmospheric Deposition, Gas, Aerosol, Ecosystem Modeling

JAEA-Data/Code 2016-014

ガス・エアロゾル交換過程を考慮した陸域生態系モデル SOLVEG

日本原子力研究開発機構　原子力科学研究部門
原子力基礎工学研究センター　環境・放射線科学ディビジョン
堅田　元喜・太田　雅和

(2016 年 11 月 10 日　受理)

自然および人為起源の大気汚染物質（ガス・エアロゾル）の陸域生態系への移行過程を評価するために、大気中ガスやエアロゾルの乾性沈着とそれに関連する過程（氷相、植物成長、土壌有機物分解）の新しいスキームを多層大気－土壌－植生 1 次元モデル SOLVEG に導入し、これらのスキームの検証試験を様々な植生地で行ってきた。本報告では、新たにモデル化したそれぞれの過程と、改良したモデルの利用方法の詳細を記述した。この改良によって、地球温暖化や大気汚染に伴う大気－陸面間の水・エネルギー・物質循環の変化と、それが生態系に及ぼす影響の評価を調べるための「陸域生態系モデル」の基盤が完成した。

原子力科学研究所：〒319-1195　茨城県那珂郡東海村大字白方 2 番地 4

Contents

目　次

1. Introduction

Over recent decades, it is of great concern over negative impacts of climate changes and human activities on earth's terrestrial ecosystems. Atmospheric deposition and emission (i.e., atmospheric exchange) of anthropogenic materials are known as the disturbance that causes various environmental issues such as air pollution, eutrophication, acidification, and even biological diversity. However, atmospheric exchange rate is hard to estimate properly because it strongly depends on complex processes related to complicated biogeochemical interactions between atmosphere and terrestrial ecosystems, i.e., energy, water, and carbon cycles. In this context, a detailed terrestrial ecosystem model is useful for understanding above interactions for various types of the land surface.

Since last decade, we have developed the one-dimensional model for atmosphere-SOiL-VEGetation interaction SOLVEG (Nagai 2004 [1)] and Katata 2009 [2)]). The model was validated with field datasets over various land types: semi-arid deserts (Katata et al 2007 [3)]), croplands (Nagai 2002 [4)], 2003 [5)], Katata et al 2007 [3)]), rice paddy field (Katata et al 2013 [6)]), temperate grasslands (Nagai 2005 [7)], Ota et al 2013 [8)]), and forests (Nagai 2003 [5)], Katata et al 2008 [9)], 2011 [10)], 2014 [11)]). In the above studies, the authors primarily focused on modeling of atmospheric deposition of gases and aerosols (Katata et al. 2011 [10)], 2013 [6)], and 2014 [11)]). Further modifications in biogeochemical interactions were also made in the model (Ota et al 2013 [8)], Desai et al., 2016 [12)]). However, a full description of model improvement in independent studies is still not available elsewhere.

Thus, the objective of the present report is to summarize new schemes incorporated in SOLVEG extended to the so-called terrestrial ecosystem model.

2. Model overview

The SOLVEG model consists of one-dimensional multi-layer sub-models for atmosphere, soil, and vegetation with a radiation transfer scheme for calculating the transmission of solar and long-wave radiation fluxes in the canopy layer. The variables from the bottom of soil layer to the top of atmospheric layer were integrated numerically using an implicit finite difference method and Gaussian elimination method. A detailed description of basic equations and model framework is found in Nagai (2004) [1] and Katata (2009) [2].

Figure 1-1 shows the schematic illustration of newly modelled processes in our recent studies. The above processes consist of dry deposition and emission of gases and aerosols, snow accumulation and melting, soil freeze-thaw, vegetation growth, and soil organic carbon cycle. The modelled equations will be described in the following chapters.

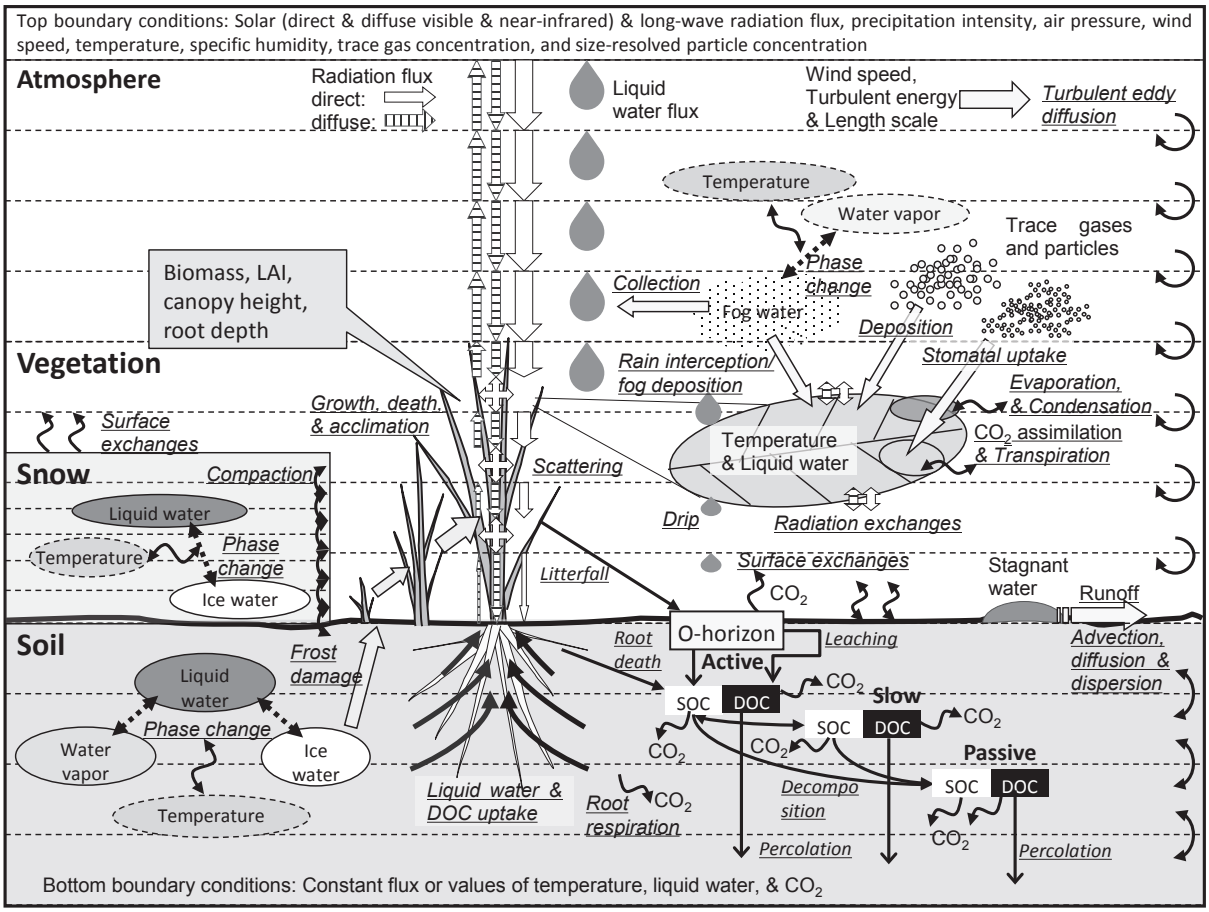

Fig.1-1 Schematic illustration of newly modelled processes in the atmosphere-soil-vegetation system represented in SOLVEG after Katata (2009) [2].

3. Atmospheric gas and aerosol exchange processes

3.1. Basic equation of atmospheric sub-model

The atmosphere sub-model calculates variables at each atmospheric layer by numerically solving one-dimensional diffusion equations for the horizontal wind speed components, potential temperature, specific humidity, liquid water content of fog, turbulent kinetic energy and length scale, and gas and particle concentrations. By using ϕ for these variables, one-dimensional diffusion equations are described in the same form as

$$\frac{\partial \phi}{\partial t} = \frac{\partial}{\partial z}\left(K_z \frac{\partial \phi}{\partial z} \right) + F_\phi , \tag{3-1}$$

where t is the time [s], z the height in the atmosphere [m], K_z the vertical turbulence diffusivity [$m^2\ s^{-1}$] calculated by the second-order turbulence closure model. The last term F_ϕ is a forcing term which includes the exchange between the vegetation and canopy air as the volume source/sink for each atmospheric variable. The top boundary conditions are provided from input data. The soil surface boundary conditions are the momentum, heat, and water vapor fluxes calculated using bulk transfer equations of wind speed, potential temperature, and specific humidity at the lowest air layer and the soil surface temperature and specific humidity, which are determined with the soil sub-model. Temporal changes in vertical profiles of typical inorganic gas (ozone, NO, NO_2, HNO_3, HCl, SO_2, and NH_3) and aerosol mass concentrations are also predicted by solving Eq. (3-1).

3.2. Dry deposition of insoluble gases

Atmospheric gases are vertically transported by turbulent eddy diffusion and mainly absorbed by plants due to stomata uptake at plants' leaves. When the plant's leaves are not wet, the source/sink term for water vapor, F_q, is represented as the aggregation of the evaporation rate of leaf surface water, E_d, and the transpiration rate, E_s, at each canopy layer as (Nagai 2004 [1])

$$F_q = a\left(E_d + E_s\right)/\rho , \tag{3-2}$$

$$E_s = \rho \frac{r_d}{R'}\left[q_{sat}\left(T_c\right) - q_a\right], \tag{3-3}$$

and

$$E_d = \rho \frac{r_s}{R'}\left[q_{sat}\left(T_c\right) - q_a\right], \tag{3-4}$$

where r_a, r_d, and r_s are the resistances [$m\ s^{-1}$] of leaf boundary layer, of evaporation of leaf surface water, and of stomata, respectively, $R' = r_a r_s + r_a r_d + r_s r_d$, $q_{sat}(T_c)$ the saturated specific humidity [$kg\ kg^{-1}$] for T_c [K], and q_a the specific humidity of air [$kg\ kg^{-1}$], respectively. Note that the resistance (r_b) and the sum of r_d and r_s are in series, but r_d and r_s are in parallel, because evaporation of the leaf surface water and transpiration occur independently from the leaf surface water and the stomata, respectively.

A diagram of trace gas exchanges between the atmosphere and the land surface is represented based on the analogy of evaporation rate as Eqs. (3-2) and (3-4). The gas deposition rate at each canopy layer, F_g [μg m^{-2} s^{-1}], is modeled using the stomatal resistance (r_s) calculated and quasi-laminar resistance over the leaves (r_a) as (Katata et al. 2011 [10])

$$F_g = a\left(D_g / D_w\right)\left(r_a + r_s\right)^{-1}\left(c_{ga} - c_{gs}\right), \tag{3-5}$$

where D_g and D_w are the diffusivity [m^2 s^{-1}] of trace gas and water vapor, and c_{ga} and c_{gs} the gas concentration [μg m^{-3}] around the leaf surface and within the stomata, respectively.

For relatively insoluble gas species such as ozone, and nitrogen monoxide (NO) and dioxide (NO_2), the gas concentration in sub-stomatal cavity is simply assumed to be zero, i.e., c_{gs} = 0 (Fig. 3-1a). This assumption has been validated by comparing calculations with observations from datasets for ozone deposition onto maize crops and broad-leaved forest canopies[10].

In addition to the above assumption of c_{gs} = 0, the stomatal resistance of r_s is set to be zero for highly reactive and water-soluble gas species of nitric acid vapor (HNO_3) and HCl (Fig. 3-1b), i.e., perfectly absorption by plant canopies. This assumption has been reported by a number of measurements (e.g., Huebert and Robert 1985 [13]).

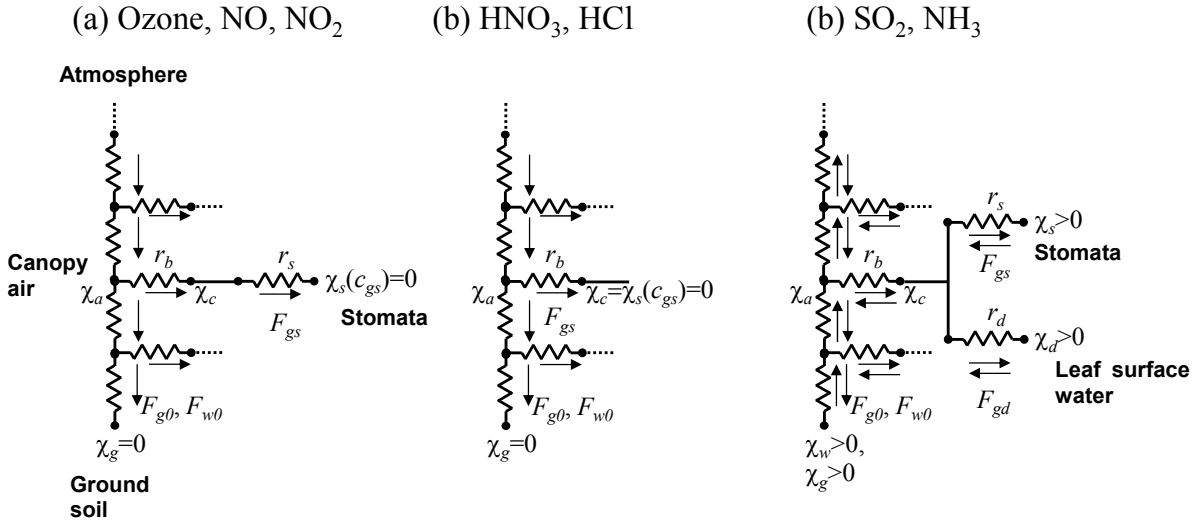

Fig.3-1 Schematic illustration of modelled processes in the atmosphere-soil-vegetation system represented in SOLVEG.

3.3. Water-soluble gas exchanges over wet canopy

Some of water-soluble gas species such as sulfur dioxide (SO_2) and ammonia (NH_3) have also other transfer pathways to the vegetative surfaces: for example, the cuticle and wetted surfaces of leaves (especially for water-soluble compounds), the branches, the trunks, and the soil exposed to atmosphere. All of these pathways, which are often

summarized as the so-called 'non-stomatal deposition', have become recognized as a sink of gases at the terrestrial surface.

When the plant nitrogen status is high at the fertilized surface, NH_3 deposition often occurs onto the wet canopy at night, but there are emissions during the daytime due to evaporation from the stomata under warm conditions. In such situations, the original model underestimated NH_3 flux over a wet canopy. Moreover, the assumption of $c_{gs} = 0$ in Eq. (3-5) is not valid for NH_3 in many cases because NH_3 has emission potentials at the foliage.

Thus, the water vapor flux over a leaf surface in SOLVEG was used to calculate NH_3 and SO_2 fluxes for each canopy layer as shown in Fig. 3-1c (Katata et al. 2013 [6]). Eqs. (3-2) and (3-3) are based on the assumption that water vapor both in the stomata and just above the leaf surface water (i.e., compensation points) are equal to the saturated value (q_{sat}) for a given leaf temperature (T_c). Using the compensation points for other trace gases in the sub-stomatal cavity (χ_s [μg m^{-3}]) and above the leaf water surface (χ_d [μg m^{-3}]) in place of q_{sat}, Eqs. (3-2) and (3-3) can be generalized for bi-directional gas exchange fluxes over stomata (F_{gs} [μg m^{-2} s^{-1}]) and leaf water surfaces (F_{gd} [μg m^{-2} s^{-1}]) as:

$$F_{gs} = a\left(D_g / D_w\right)R'^{-1}\left[\left(r_b + r_d\right)\chi_s - r_b\chi_d - r_d\chi_a\right], \tag{3-6}$$

and

$$F_{gd} = a\left(D_g / D_w\right)R'^{-1}\left[\left(r_b + r_s\right)\chi_d - r_b\chi_s - r_s\chi_a\right], \tag{3-7}$$

where χ_a is the ambient gas concentration [μg m^{-3}] in the canopy layer. The above equations are similar in concept to existing bi-directional NH_3 exchange models (e.g., Zhang et al. 2010 [14]). The total gas exchange flux over the leaves can be calculated as the sum of F_{gs} and F_{gd} for all canopy layers.

The bi-directional flux of NH_3 is calculated using Eqs. (15) and (16) and the calculated value of χ_s based on thermodynamic equilibrium between NH_3 in the liquid and gas phases:

$$\chi_s = \left(\frac{161500}{T_c}\right)\exp\left(-\frac{10378}{T_c}\right)\Gamma_s, \tag{3-8}$$

where χ_s is the stomatal emission potential (also known as the apoplastic ratio) at 1013 hPa, as:

$$\Gamma_s = \frac{\left[NH_4^+\right]_s}{\left[H^+\right]_s}, \tag{3-9}$$

where $[NH_4^+]_s$ and $[H^+]_s$ are the NH_4^+ and H^+ concentrations [mol L^{-1}] in the apoplastic fluid, respectively. $[H^+]_s$ is defined as 10^{-pH}, where the pH of the apoplastic fluid is given at 1013 hPa.

In these calculations, when the canopy is wet with microscopic water layers that appear under high relative humidity condition (RH > 60%), water-soluble gases can also be

emitted from wet canopies through evaporation. For simplification, some models have assumed that the NH_3 concentration at the leaf surface is zero for transfer between the canopy air space and the leaf surface. In the modified SOLVEG model, the NH_3 concentration at the leaf surface water (χ_d) was calculated by assuming Henry's Law and dissociation equilibrium with the atmospheric concentration of NH_3 at each canopy layer. To calculate the exchange flux of NH_3 and SO_2 over the wet canopy, the following formula for the evaporation (cuticular) resistance (r_d) was applied:

$$r_d = 31.5AR^{-1}\exp\left[a\left(100 - RH\right)\right], \tag{3-10}$$

where AR is the ratio of total acid/NH_3, represented as $(2[SO_2] + [HNO_3^-] + [HCl])/[NH_3]$, and RH the relative humidity [%] at each atmospheric layer calculated using the diffusion equation for specific humidity (Nagai 2004 [1)]). The value of AR is calculated from calculations of gaseous inorganic concentration at each atmospheric layer. Since the affinity of SO_2 for the leaf surface was approximately twice that of NH_3 (van Hove et al. 1989 [15)]), a half value of r_d calculated by (3-10) is applied to SO_2 deposition.

3.4. Dry deposition of aerosols

The atmosphere and vegetation sub-models include the module for the calculation of fog deposition onto the leaves based on the processes of inertial impaction and gravitational settling of particles at each vegetation layer (Katata 2009 [2)]). In the present study, a novel scheme of the collection rates due to Brownian diffusion and interception, which can affect fine particles typically smaller than 0.1 μm in diameter, is developed (Katata et al. 2011 [10)]). Both processes are formulated based on semi-empirical equations obtained by wind-tunnel studies for packed fibres of a filter.

The particle deposition rate, F_p [μg m^{-2} s^{-1}], in each canopy layer is represented as

$$F_p = aE_p, \tag{3-11}$$

and

$$E_p = \varepsilon F_f |\mathrm{u}| c_p, \tag{3-12}$$

where E_p is the capture of particles by leaves [μg m^{-3} s^{-1}], ε the total capture efficiency of the plants' leaves for particles, F_f the shielding coefficient for particles in horizontal direction, $|\mathbf{u}|$ the horizontal wind speed [m s^{-1}] at each canopy layer, and c_p the mass concentration of aerosol particles [μg m^{-3}].

Assuming that each collection mechanism acts in series, the total capture efficiency ε can be expressed as

$$\varepsilon = 1 - \prod_x \left(1 - \varepsilon_x\right), \tag{3-13}$$

where x is the collection mechanism of inertial impaction, gravitational settling, Brownian

diffusion, and interception. Since the formulations of ε for inertial impaction ε_{imp} and gravitational settling ε_{grv} have been described in Katata (2009) [2], only collection efficiencies due to Brownian diffusion and interception are described below.

Fine particles smaller than approximately 0.1 μm diffuse toward the foliar surface (Brownian diffusion), when moving along the streamline around the leaves under forced convection. The collection efficiency due to Brownian diffusion, ε_{df}, is described by the following formula

$$\varepsilon_{df} = 2.7Pe^{-2/3}, \tag{3-14}$$

and

$$Pe = \frac{|u| d_{leaf}}{D_B(d_p)}, \tag{3-15}$$

where Pe is the Peclet number, which is the product of Schmidt (Sc) and Reynolds number (Re), d_{leaf} the characteristic length of vegetation element [m] (e.g., needle diameter for coniferous forest), and $D_B(d_p)$ the Brownian diffusion coefficient [m^2 s^{-1}] as a function of particle diameter d_p [μm]. The value of 2.7 in Eq. (3-14) is a number determined by experimental measurements of filter efficiencies. Equation (3-14) includes both effects of convection (Re) and particle diffusion (Sc) and is physically more reasonable than the prior parameterizations using only Sc in the commonly used model such as Zhang et al. (2001) [16].

When small particles perfectly follow a streamline that happens to come within one particle radius of the foliar surface, the particle hits the leaf and is captured because of its finite size (interception). When small particles perfectly follow a streamline that reaches within one particle radius of the foliar surface, the particle hits the leaf and is captured because of its finite size (interception). The collection efficiency due to interception, $\varepsilon_{in,i}$, is expressed as

$$\varepsilon_{in} = (1 + R_i) - (1 + R_i)^{-1}, \tag{3-16}$$

and

$$R_i = \frac{d_p}{d_{leaf}}, \tag{3-17}$$

where R_i and $d_{p,i}$ are the dimensionless parameter of interception and the (wet) particle diameter [m] of the bin, respectively. For broad-leaved trees (planar obstacles), the parameter R is modified based on an analytical formulation of the collection velocity for a Dirac distribution of the leaf width as

$$R_i = \frac{d_p}{d_{leaf}}\left(2 + \ln\frac{4d_{leaf}}{d_p}\right). \tag{3-18}$$

3.5. Aerosol hygroscopic growth

Hygroscopic growth is significant in aerosols containing water-soluble compounds such as ammonium sulfate under humid conditions. The degree of water uptake by aerosols is typically represented by the hygroscopic growth factor, G_f, defined as the ratio between the humidified and dry particle diameters. In SOLVEG, the widely used κ-Köhler theory (Petters and Kreidenweis 2007 [17]) was employed to calculate the water uptake of aerosols in the atmosphere, i.e., the wet diameter of particles in each bin, d_p. The theory is convenient as it requires only one parameter κ to represent the hygroscopicity of a single particle as internal mixtures of inorganics and organics. According to Petters and Kreidenweis (2007) [17], the typical experimental values of κ for both ammonium sulfate and ammonium nitrate are 0.6, the sodium chloride and sodium bisulfate values are 1.0 and the values for hygroscopic organic compounds such as organic acids are in the range of 0.1–0.2. Using the above κ values and available data for inorganic compounds, the hygroscopicity of a multi-component particle was calculated by a volume-weight average of κ for each compound.

For larger particles (d_p>1 μm), the mass transfer of water vapor during particle growth restricts hygroscopic growth because the particles require several minutes to several ten minutes to reach equilibrium, especially under near-saturated conditions. Mass transfer of water vapor to the aerosol surface is dynamically calculated for each time step in SOLVEG as follows (Katata et al. 2014 [11])

$$\frac{dL_{a,i}}{dt} = \frac{\pi}{4}\alpha \bar{c} d_p^{\,2} f(d_p, \alpha) n \rho \left(q - q_{eq}\right), \tag{3-19}$$

where L_a and n are the total aerosol water content [kg m^{-3}] and the number concentration [m^{-3}] of each bin, q [kg kg^{-1}] is the water vapor mixing ratio in the canopy layer, $\bar{c}$ [m s^{-1}] is the molecular speed of the water vapor, α is the mass accommodation coefficient, which is set to unity, and q_{eq} [kg kg^{-1}] and κ are the equilibrium water vapor mixing ratio for the aerosol surface of the bin and the hygroscopicity of particles, as determined by the κ-Köhler theory. The correction factor, f, for the transition regime is taken from Fuchs and Sutugin (1971) [18]. For simplicity, we assumed a single log-normal function for aerosol size distributions without size dependencies of the aerosol properties, i.e., κ and the volume fraction of inorganic compounds (f_{io}), is unchanged with particle size. The procedure used to determine the number concentration of each bin, n, and to integrate the mass transfer equation, Eq. (3-19), was calculated as follows. First, the total aerosol mass was calculated from inorganic components measured by filter pack, the above volume fractions of the total inorganics, and an assumed particle density, 1.8 kg m^{-3}. Then, n in Eq. (3-19) was calculated for each bin and was integrated for a given log-normal size distribution with given parameters of the number-equivalent geometric mean dry diameter (d_{gn} [μm]) and the geometric standard deviation (σ_g).

In Eq. (3-19), the mass transfer of heat is not calculated. The water vapor mixing ratio, q, is assumed to be constant during particle growth and shrinkage due to water uptake. This assumption is reasonable because the maximum calculated total aerosol water mixing ratio is less than 1% of q.

It should be noted that the κ-Köhler theory does not take into account the water hysteresis effect, i.e., the efflorescence and deliquescence of aerosols. The authors investigate the impact of this effect via test calculations of the aerosol thermodynamic equilibrium model ISORROPIA2 (Fountoukis and Nenes 2007 [19]) at Japanese broad-leaved forest in summertime [11]. The results showed that the aerosol water content is greater than zero throughout the simulation period; i.e, the RH was always larger than the mutual deliquescence relative humidity (MDRH) of the aerosols. Thus, the scheme based on the κ-Köhler theory is applicable to typical humid temperate climate.

Using the total liquid water content, L_a [kg m^{-3}], the growth factor for bin, G_f, can be calculated as

$$G_f = \frac{d_p}{d_{pdry}} = \frac{\left[\frac{6L_a}{\pi\rho_w} + \left(d_{pdry}\right)^3\right]^{\frac{1}{3}}}{d_{pdry}}, \qquad (3\text{-}20)$$

where d_{pdry} is the dry diameter of the particles [m] and ρ_w is the density of water [kg m^{-3}]. Finally, the mean growth factor, G_{fave}, is calculated by volume-averaging G_f in Eq. (3-20) for all bins.

Figure 3-2 shows an example of calculations in daytime averaged size-resolved deposition velocity compared with data from the literature. Literature values showed that the size-resolved deposition velocity over the broad-leaved forests increased with an increase in particle size, while the data are highly scattered from 0.1 to 1 cm s^{-1}. The model reproduced this tendency, and the calculated values were at least within the range of measured values. However, underestimations still remain in the calculations because the model does not include additional particle deposition processes due to thermophoresis, diffusiophoresis and the Stefan flow effect, turbophoresis, or electrophoresis. Further improvements of the model and evaluations with more detailed datasets are required.

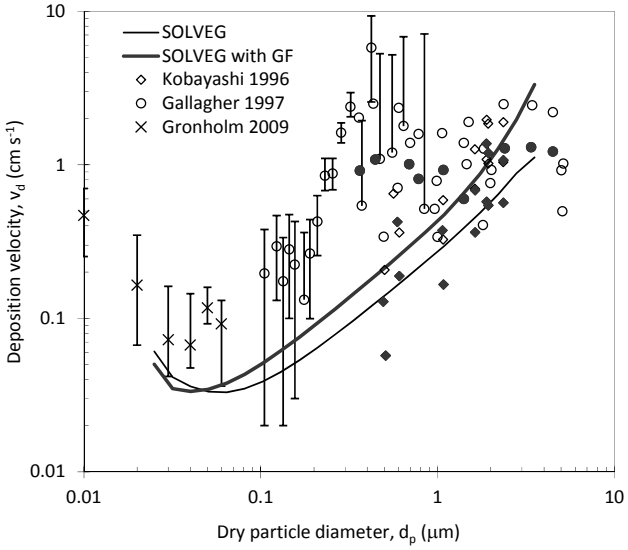

Fig.3-2 Size-resolved dry deposition velocity calculated by the model (d_{gn}=0.2 μm, σ_g=1.6) with (κ=0.6; red solid lines) and without particle growth (black solid lines) over the Japanese broad-leaved forest (after Katata et al. 2014 [11]). Observational data from the literature for coniferous (open plots) and broad-leaved forests (closed plots) are plotted.

4. Other processes for terrestrial ecosystem modeling

4.1. Snow accumulation and melting

The ice phase processes in snow and soil layers have an important role in water cycle in the terrestrial ecosystem under cold environment. To simulate these processes, the multi-layer snow module is incorporated into the model. Most of variables in the following equations are based on either the Community Land Model, CLM (Oleson et al. 2010 [20]) or SNTHERM (Jordan 1991 [21]), while the model is unique in including the gravitational and capillary liquid water flows in unsaturated snow based on van Genuchten's concept (c.f., Hirashima et al 2010 [22]).

The temporal change in snow temperature T_{sn} [K] is expressed by the heat conduction equation based on Yamazaki (2001) [23] as

$$C_{sn}\rho_{sn}\frac{\partial T_{sn}}{\partial t}=\frac{\partial}{\partial z}\left(\lambda_{sn}\frac{\partial T_{sn}}{\partial z}\right)-\frac{\partial I_n}{\partial z}-l_f E_{smel}-lE_{sb}\,, \tag{4-1}$$

where C_{sn} and ρ_{sn} the specific heat of snow [J kg^{-1} K^{-1}] and the density of the bulk snow [kg m^{-3}], respectively, λ_{sn} the thermal conductivity of snow [Wm^{-1}K^{-1}], I_n the net solar flux in snow [W m^{-2}], l_f and l the latent heats of fusion and sublimation [J kg^{-1}] , respectively, and E_{smel} the melting or freezing rate in snow [kg m^{-3} s^{-1}], and E_{sb} the sublimation rate of water vapor in snow [kg m^{-3} s^{-1}]. I_n is calculated as $(1-r)(1-A_b)S_{down}\exp(-\mu z)$, where r the absorptivity of solar radiation at the snow surface, A_b the snow albedo as a sum of that for direct and diffuse visible and near-infrared solar and long-wave radiations (Fig. 2-1) (Wiscombe and Warren 1980 [24]), and μ the extinction coefficient of solar radiation (Jordan 1991).

E_{sb} is calculated only at the snow surface by assuming that water vapor is saturated over the snow

$$E_{sb0}=\sigma_{sn}\rho c_{E0}|\mathrm{u}|\left[q_{sat}(T_{sn0})-q_r\right], \tag{4-2}$$

where σ_{sn} is the fractional area of snowcover parameterized using physical snow height (Essery et al. 2013 [25]), ρ the density of air [kg m^{-3}], c_{E0} the bulk coefficient, $q_{sat}(T_{sn0})$ the saturated specific humidity at the snow surface temperature [kg kg^{-1}], T_{sn0} the snow surface temperature [K], and $\boldsymbol{u}$ and q_r the horizontal wind speed [m s^{-1}] and specific humidity [kg kg^{-1}] at the lowest atmospheric layer, respectively.

Melting or freezing rate in snow is calculated by snow temperature as

$$E_{smel}=\frac{C_{sn}\rho_{sn}}{l_f}\frac{T_{sn}-T_m}{\partial t}, \tag{4-3}$$

where T_m is the melting point of 273.15 K. Using E_{smel}, ice content in snow w_i at each snow layer [kg m^{-2}] is determined as

$$\frac{\partial w_i}{\partial t}=-E_{smel}\Delta z\,. \tag{4-4}$$

The mass balance equation for liquid water in snow is given as

$$\rho_w \frac{\partial \eta_{sw}}{\partial t} = \frac{\partial}{\partial z}\left(D_{sw} \frac{\partial \eta_{sw}}{\partial z} + K_{sw} \right) - E_{smel}, \tag{4-5}$$

where η_{sw} is the snow volumetric liquid water content [$m^3\ m^{-3}$], D_{sw} is the snow liquid water diffusivity [$m^2\ s^{-1}$], K_{sw} the snow unsaturated hydraulic conductivity [$m\ s^{-1}$], and ρ_w the density of liquid water [$kg\ m^{-3}$]. The equations for D_{sw} and K_{sw} are similar to those for soil water content in capillary region (Katata 2009) using the empirical parameters given by Hirashima et al. (2010) [22].

Snow accumulation and compaction at each snow layer are modelled as

$$\frac{1}{\Delta z}\frac{\partial \Delta z}{\partial t} = C_{snf} - C_{met} - C_{over} - C_{mel}, \tag{4-6}$$

$$C_{met} = c_1 \exp\left[-c_2 \left(T_m - T_s \right) - c_3 \max\left(0, \rho_s - \rho_0 \right) \right], \tag{4-7}$$

$$C_{over} = \frac{-P_s}{\eta_{sn}}, \tag{4-8}$$

and $$C_{mel} = -\frac{1}{\Delta t}\max\left(0, \frac{f_{ice} - f_{ice}^{+}}{f_{ice}} \right), \tag{4-9}$$

where Δz is the snow layer thickness [m], C_{snf}, C_{met}, C_{over}, and C_{mel}, the change rate in Δz [s^{-1}] due to snowfall, metamorphism, overburden, and melting, respectively, and f_{ice} and f_{ice}^{+} the fraction of ice before and after the melting, respectively. C_{snf} is calculated as $S_f\ \rho_{fs} / \rho_w$, where S_f is the snowfall rate [$mm\ s^{-1}$] given by either the input data or the empirical equation using total rainfall rate and wet bulb temperature (Yamazaki 2001 [23]), and ρ_{fs} the fresh snow density [$kg\ m^{-3}$] obtained by Boone (2002) [26]. Values for the parameters in the above equations are given by Oleson et al. (2010) [20].

Snow grain growth is calculated based on Jordan (1991) [21] as

$$\frac{\partial d_{sn}}{\partial t} = \begin{cases} \dfrac{g_1 \left| U_v \right|}{d_{sn}} & \eta_{sw} = \eta_{swilt} \\ \dfrac{g_2}{d_{sn}} \left(\eta_{sw} + 0.05 \right) & \eta_{swilt} < \eta_{sw} < 0.09 \\ 0.14 \dfrac{g_2}{d_{sn}} & 0.09 < \eta_{sw} \end{cases}, \tag{4-10}$$

where d_{sn} is the snow grain diameter [m], U_v the mass vapor flux in snow layer [$kg\ m^{-2}\ s^{-1}$], and g_1 and g_2 the parameters. The formulation of U_v and values of g_1 and g_2 are given by Jordan (1991) [21].

After the above calculations for temperature, and liquid and ice water contents, and accumulation and compaction in snow, the number of snow layers is adjusted by either combining or subdividing layers (Jordan 1991 [21]) to obtain the physical snow height.

4.2. Soil freeze-thaw

In the soil module, freeze-thaw processes in soil are considered to heat conduction and liquid water flow equations as follows

$$C_s\rho_s\frac{\partial T_s}{\partial t}=\frac{\partial}{\partial z}\left(\lambda_s\frac{\partial T_s}{\partial z}\right)-lE_b-l_fE_{mel}, \tag{4-11}$$

and

$$\rho_w\frac{\partial \eta_w}{\partial t}=\frac{\partial}{\partial z}\left(D_w\frac{\partial \eta_w}{\partial z}+K\right)-E_b-E_{mel}, \tag{4-12}$$

where C_s and ρ_s the specific heat of soil [J kg^{-1} K^{-1}] and the density of the bulk soil [kg m^{-3}], respectively, λ_s the thermal conductivity of soil [Wm^{-1}K^{-1}], l_f and l the latent heats of fusion and sublimation [J kg^{-1}] , respectively, η_w is the volumetric soil water content [m^3 m^{-3}], D_w is the soil water diffusivity [m^2 s^{-1}], K the unsaturated hydraulic conductivity [m s^{-1}], E_b the evaporation or condensation or sublimation of soil water [kg m^{-2} s^{-1}], and E_{mel} the melting or freezing rate in soil [kg m^{-3} s^{-1}], respectively. The soil water diffusivity D_w is expressed by

$$D_w=K\frac{\partial \psi}{\partial \eta_w}, \tag{4-13}$$

where ψ is the water potential [m].

Ice content at each soil layer η_i [m^3 m^{-3}] is determined in a similar way of snow ice content [Eqs. (4-2) and (4-3)] as

$$\frac{\partial \eta_i}{\partial t}=-\frac{E_{mel}}{\rho_i}, \tag{4-14}$$

and

$$E_{mel}=\frac{C_s\rho_s}{l_f}\frac{T_s-T_m}{\partial t}, \tag{4-15}$$

where ρ_i the density of ice [kg m^{-3}].

The water potential ψ [m] and unsaturated hydraulic conductivity K [m s^{-1}] in frozen soil [Eq. (4-12)] are modeled based on the concept of freezing point depression

$$\psi=\psi_{unfrozen}\left(1+C_k\eta_i\right)^2, \tag{4-16}$$

and

$$K=K_{unfrozen}10^{-E_i\eta_i}, \tag{4-17}$$

where C_k and E_i are the empirical parameters given by Zhang et al (2007) [27], and $\psi_{unfrozen}$ and $K_{unfrozen}$ the ψ and K in unfrozen soil described in Katata (2009) [2], respectively.

After the above modification, SOLVEG can predict temporal changes in ice and liquid water content, temperature, and grain size at each snow layer, and ice water content in each soil layer.

4.3. Vegetation growth

Towards ecosystem modeling, the processes for plant phenology (e.g., leaf development and senescence) and soil and dissolved organic carbon cycle are implemented into the

SOLVEG. First, the relevant schemes in grass growth model LINtul GRAssland, LINGRA (Schapendonk et al 1998 [28], Höglind et al 2001 [29]) is coupled with the vegetation sub-model to simulate the vegetation growth. LINGRA is based on plant morphological key processes and light interception and has separated algorithms for source- and sink-related processes and a mechanistic, though simple, approach of grass morphological development, simulating the natural sequence of events in grasslands as regular defoliation due to grazing or cutting. The scheme is evaluated by using experimental datasets of harvestable dry matter of perennial rye grass collected in Europe. Since a full description of LINGRA is available in Schapendonk et al (1998) [28], the important equations are summarized below.

Total actual vegetation growth, ΔW (g d^{-1}), is determined by the balance between assimilate demand (sink), ΔW_d, and assimilate supply (source), ΔW_s. In the following, the subscript d denotes the demand function, and the subscript s denotes the supply function.

Newly formed assimilates available for growth are partitioned between the leaves (above-ground biomass) and the roots (below-ground biomass). This partitioning between leaves and roots is independent from limitation factors of the growth (i.e., sink- or source-limited). Therefore, the total assimilate demand for (sink-limited) crop growth, ΔW_d, is

$$\Delta W_d = \frac{\Delta LAI_n}{\Delta SLA \cdot f_{lv}}, \tag{4-18}$$

where ΔLAI_n [m^2 m^{-2} d^{-1}] and ΔSLA [m^2 m^{-2} g^{-1}] are the daily increase in leaf area index (LAI) and the specific leaf weight of the newly formed leaves, respectively, and f_{lv} the fraction of assimilates that is partitioned to the leaves. Currently, f_{lv} is set to unity based on the assumption that all available carbon is preferentially allocated to leaves, and the rest of carbon in the reserve ΔW_{pool} in Eq. (4-20) is partitioned to root growth. This assumption may be valid for typical perennial grasslands (Höglind et al 2001 [29]).

There are two sources of assimilate supply ΔW_s [g m^{-2} d^{-1})] the amount of assimilates fixed by photosynthesis during the day, P [g-C m^{-2} d^{-1}] and the reallocated assimilates from the amount of carbohydrates stored in the reserve pool (i.e. stubble), ΔW_{pool} [g-C m^{-2} d^{-1}].

$$\Delta W_s = P + \Delta W_{pool}, \tag{4-19}$$

where P is calculated as accumulation of the net assimilation for each time step in vegetation sub-model (Nagai 2004 [1]). In the calculation of P, the cold acclimation depending on seasonal air temperature variation is considered via decreasing the maximum catalytic capacity of Rubisco (V_{cmax}) by simply multiplying the factors of annual change of photosynthesis (Mäkelä et al 2004 [30]). When snow covers grasses, no photosynthesis is assumed due to low light availability and only soil respiration is considered.

Actual total crop growth rate ΔW is the minimum of the assimilate demand and the assimilate supply as $\min(\Delta W_d, \Delta W_s)$. Thus, growth takes only place when the supply

(photosynthesis plus reallocation from the reserve pool) exceeds or equals the demand function. Conversely, carbohydrates will be stored in the reserve pool ΔW_{pool} when the photosynthetic supply (ΔW_s) exceeds the demand (ΔW_d) as

$$\Delta W_{pool} = \Delta W_s - \Delta W_d \,. \tag{4-20}$$

Net leaf growth of LAI, ΔLAI [m^2 m^{-2} d^{-1}], is derived from the amount of assimilates available for growth and the death rate of leaves by senescence as

$$\Delta LAI = \Delta LAI_n - \Delta LAI_d \,, \tag{4-21}$$

where ΔLAI_d [m^2 m^{-2} d^{-1}] is the death rate of leaves calculated from a relative death rate due to internal shading and by water stress. The LAI value updated with ΔLAI is applied to the vegetation sub-model.

Natural turnover of leaves and roots are modeled using typical life spans in years (Arora and Boer 2005 [31]). The fraction of roots in soil layers and rooting depth are modeled as a function of root biomass (Arora and Boer 2003 [32]).

It is noted that the vegetation growth scheme implemented here is currently available for only grassland ecosystem. Further modification of the allocation scheme is required so that the model is applied to forest ecosystems.

4.4. Soil organic carbon cycle

The soil sub-model has been updated to simulate the organic matter decomposition and dissolved organic carbon (DOC) leaching in the aboveground litter layer, the belowground input of carbon from roots, and soil organic carbon (SOC) turnover and DOC transport along water flows throughout the soil profile for three SOC pools (active, slow, and passive, characterized by a turnover time of years, decades, and millennia, respectively) (Ota et al. 2013 [8]). For these three SOC pools, it was assumed that at every time step and every grid within the soil, an immediate equilibrium can be achieved for sorption and desorption of soil C between the solid (SOC contained in the soil constituents) and dissolved (DOC contained in the soil water) phases.

The change in the SOC content for the ith C pool (subscript i=1, 2, and 3 for the active, slow, and passive carbon, respectively) at a certain depth in the soil profile is modeled by

$$\frac{\partial \rho_b \chi_{ss,i}}{\partial t} = S_{ss,i} - k_{ss,i} \rho_b \chi_{ss,i} \,, \tag{4-22}$$

where ρ_b is the dry bulk density of the soil [kg m^{-3}], $S_{ss,i}$ the input rate of carbon as SOC into the ith SOC pool [kg-C m^{-3} s^{-1}], and $\chi_{ss,i}$ and $k_{ss,i}$ the SOC content per dry soil mass [kg-C kg^{-1}] and the decomposition rate of the SOC [yr^{-1}] in the ith carbon pool. At the ground surface, dead leaf biomass calculated by ΔLAI_d and the specific leaf weight in section 4.3 is used as input to the aboveground litter layer.

The transport of DOC for the *i*th carbon pool in the soil is then modeled by considering the diffusion and advection of the DOC, as well as the loss of DOC via root-water uptake and microbial decomposition as

$$\frac{\partial \eta_w \chi_{sw,i}}{\partial t} = \frac{\partial}{\partial z}\left(D_{wsw} \frac{\partial \chi_{sw,i}}{\partial z} \right) - \frac{\partial E_w \chi_{sw,i}}{\partial z} - e_r \chi_{sw,i} - k_{sw,i} \eta_w \chi_{sw,i}, \qquad (4\text{-}23)$$

where D_{wsw} is the effective diffusivity of the DOC [m^2 s^{-1}], E_w the vertical soil water flux [m^3 m^{-2} s^{-1}], e_r the root-water uptake [m^3 m^{-3} s^{-1}], and $k_{sw,i}$ the decomposition rate for DOC defined according to each DOC pool [s^{-1}]. η_w, E_w, and e_r at each soil layer are calculated in the soil sub-model (Katata 2009 [2)]).

An example of parameter settings of the sub-models described in the section is shown in Table 4-1.

Table 4-1 An example of parameter settings of SOLVEG for alpine grassland ecosystem (Desai et al. 2016 [12]).

Description	Unit	Value
Initial carbohydrate storage	kgDM ha^{-1}	2100
Maximum catalytic capacity of Rubisco at 25 ˚C	μmol m^{-2} s^{-1}	60
Initial tiller density	number m^{-2}	600
Dark respiration rate of leaves at 25 ˚C	μmol m^{-2} s^{-1}	1.2
Activation energy for dark respiration	J mol^{-1}	134.6
Minimum stomatal conductance	mol m^{-2} s^{-1}	0.0219
Initial leaf area index (LAI)	m^2 m^{-2}	2.0
Initial root biomass	kgDM ha^{-1}	5000
Slope of stomatal conductivity in response to assimilation	–	9
Phyllochron (interval between leaf appearance)	˚C day	70
Leaf life span	year	1.5
Root life span	year	1.0
Maximum drought leaf loss rate	day^{-1}	0.005
Shape parameter for leaf loss due to drought	–	3
Maximum storage carbohydrate fraction	gDM gDM^{-1}	0.3
Time constant for storage carbohydrate	day	1
Specific leaf area (SLA)	m^2 $kgDW^{-1}$	10
Maximum LAI-induced leaf loss rate	day^{-1}	0.06
Minimum threshold temperature for leaf appearance and tillering	˚C	5
Maximum threshold temperature for leaf appearance and tillering	˚C	10
LAI after the grass cut	m^2 m^{-2}	0.8
Parameters for soil microbiological module		
Snow layer thickness	mm	5
Parameter for the effect of soil specific surface on matric potential due to the presence of ice	–	8
Irreducible liquid water content in snow	m^3 m^{-3}	0.03

5. Model code

The model code is written in fortran77 and 90, and executable on over Linux/Unix and Cygwin (Windows) environments. Details of the model code and procedure to run the model are described here. Note that underlined files represent newly incorporated routines in the present study. Flow chart is illustrated in Fig. 5-1.

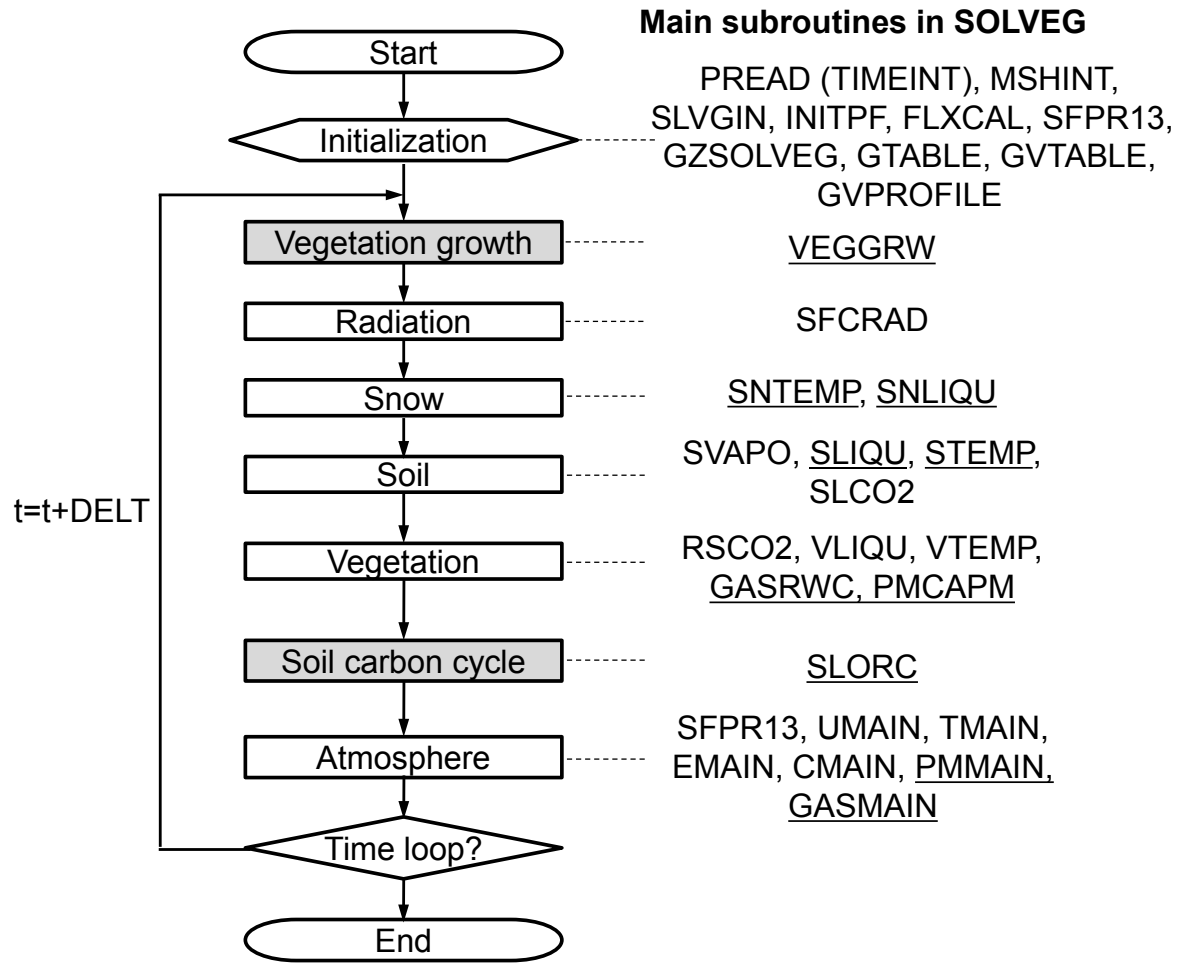

Fig. 5-1 Calculation flow chart of the terrestrial ecosystem model SOLVEG. Two subroutines for vegetation growth and soil carbon cycle are calculated on a day (grey shaded boxes), while other ones are calculated every time step (DELT). Newly incorporated and modified subroutines are underlined in the figure.

5.1. Structure of model code

The SOLVEG model mainly consists of four directories for the source code (SRC), input data as upper boundary conditions (INPUT), tables (TABLE), and output data (OUTPUT) under the root directory (SOLVEG). Each directory contains the following files:

a) Root: SOLVEG/

- Shell-script for execution go_1D.sh

b) Main source code: SOLVEG/SRC/

- Shell-script for compilation — Makefile
- Executable file — solveg
- Module files (prm_*)
  - prm_grid.f — Common grid parameters
  - prm_var.f — Common constants
  - prm_array.f — Common array variables (call prm_grid and prm_var)
  - prm_gasspc.f — Molecular weight for gas species
  - prm_iospc.f — Parameters for inorganic aerosol species
  - prm_nrspc.f — Molecular weight for non-photochemical reactive gas species
  - prm_snfz.f — Parameters for snow and soil freeze-thaw
  - prm_soil.f — Parameters for dry soil condition
  - prm_veg.f — Parameters for vegetation growth
- Program files (*.f)
  - efalbedo.f — Subroutine EALBED: soil surface albedo
  - ehws.f — Subroutine EHWS: saturated soil water content
  - eli2va.f — Subroutine ELI2VA: specific humidity in soil pore
  - eppara.f — Subroutine EPPARA: leaf projection coefficient
  - espara.f — Subroutine ESPARA: soil heat capacity and conductivity
  - evpara.f — Subroutine EVPARA: soil vapor diffusivity/evaporation resistance
  - ewpara.f — Subroutine EWPARA: soil water conductivity and diffusivity
  - faipsy.f — Functions FAIM, FAIH, PSYM, PSYH, SHMD, and SHMDD: soil surface exchange functions
  - fcpair.f — Function FCPAIR: specific heat of air
  - fcw.f — Function FCW: specific heat of water
  - fdensa.f — Function FDENSA: air density
  - fl.f — Function FL: latent heat of vaporization
  - gtable.f — Subroutine GTABLE: soil parameters
  - gvprofile.f — Subroutine GVPROFILE: vegetation profile data
  - gvtable.f — Subroutine GVTABLE: vegetation parameters
  - gzsolveg.f — Subroutine GZSOLVEG: soil and vegetation grid
  - lineint.f — Subroutine LINEINT: linear interpolation of data
  - main.f — Main routine SOLVEG
  - pdebugw0.f — Subroutine DEBUGW: atmospheric variable output
  - pfluxcal.f — Subroutines SFPR13, FLXCAL, KMHCAL, and SAVEOD: turbulence and variable for the next time step
  - pgener.f — Subroutines GENER, DIREC1, and DIREC2: diffusion scheme

- pinit01.f Subroutine MSHINT: atmosphere grid
- pinitpf.f Subroutines INITPF and CLSL2A: initial atmospheric variables
- pmain03.f Subroutines UMAIN, TMAIN, EMAIN, and CMAIN: wind, temperature, specific humidity, fog water, turbulence, and CO_2 concentration profile
- ppcal.f Subroutine PCAL: air pressure
- ppread.f Subroutines PREAD: read input parameters and meteorological and atmospheric chemistry data
  Subroutine DEWTMP: dew point
- ptint.f Subroutine TIMEINT: read temporal change in meteorological and atmospheric chemistry data
- shifi1.f Subroutine HIFI1: water advection in soil
- slco2.f Subroutine SLCO2: soil CO_2
- sliqu.f Subroutine SLIQU: soil water
- solveg.f Subroutines SLVGIN and SOLVEG: soil-vegetation processes
- solver1.f Subroutine SOLV1: diffusion scheme
- solver2.f Subroutine SOLV2: diffusion scheme
- srad.f Subroutine SFCRAD: canopy radiation transmission
- sradiatn.f Subroutine RADIATION: solar and long-wave radiation
- stemp.f Subroutine STEMP: soil temperature
- svapo.f Subroutine SVAPO: specific humidity in soil pore
- svfogcp.f Subroutine FOGCAP: cloud water collection rate by leaves
- svliqu.f Subroutine VLIQU: leaf surface water and canopy water flux
- svrsco2.f Subroutine RSCO2: CO_2 assimilation and stomatal resistance
- svrsst.f Subroutine RESISTS: stomatal resistance
- svsed.f Subroutine SED and SEDPM: gravitational settling flux
- svtemp.f Subroutine VTEMP: vegetation temperature
- swadsp.f Subroutine WADSP0: dry soil processes
  Function POTEV: potential surface evaporation

c) Program files (*.f) for gas and particle dry deposition: SOLVEG/SRC/GAS-PM

- fdist.f Function FDIST, DGL10, NORM, and DEIR: fogwater size distribution
- feps.f Function EPS and BETA: Fogwater and aerosol capture efficiency
- fvgrv.f Function VGRV: gravitational settling function
- gfkappa.f Soubroutine GFKAPPA, GET_D_WET, and ET_RH_EQ: aerosol hygroscopisity
- hlconst.f Function HLCONST: Henry's law constant

- pgasmain.f Soubroutine GASMAIN: gas concentration profile for each chemical species
- pmmain.f Soubroutine PMMAIN: aerosol concentration profile for each chemical species and mode
- svgasrwc.f Soubroutine GASRWC: gas transfer resistance
- svpmcpm.f Soubroutine PMCAPM: aerosol mass collection rate by leaves

d) Program files (*.f) for snow: SOLVEG/SRC/SNOW

- faipsysn.f Function FAIMS, FAIHS, PSYMS, and PSYHS: snow surface exchange functions
- snliqu.f Subroutine SNLIQU: snow water content
- snpara.f Subroutine SNPARA: snow heat capacity and conductivity
- sntemp.f Subroutine SNTEMP: snow temperature
- snwpara.f Subroutine SNWPARA: snow water conductivity and diffusivity
- solver1sn.f Subroutine SOLV1SN: diffusion scheme for snow
- solver2sn.f Subroutine SOLV2SN: diffusion scheme for snow

e) Program files (*.f) for vegetation growth and SOC/DOC: SOLVEG/SRC/VEG_SOC

- slorc.f Subroutine SLORC: soil organic carbon cycle
- veggrw.f Subroutine VEGGRW: vegetation growth
  Subroutine TILSUB: tillering
  Subroutine MOWING: mowing
  Subroutine FATALERR and function LINT2, FCNSW, INSW, LIMIT, NOTNUL, REAAND, ILENG, and INTGRL: functions

f) Input data: SOLVEG/INPUT/

- Meteorological data file (fort.9) metdata.dat (interval of TINTINP)
- Fine aerosol data file (fort.11) fpmdata.dat (unequal time interval)
- Coarse aerosol data file (fort.12) cpmdata.dat (unequal time interval)
- Gas concentration data file (fort.13) gasdata.dat (unequal time interval)

g) Tables: SOLVEG/PARAMETER/

- Parameter file (fort.10) param_1D
- Vertical grid coordinate file (fort.14) zmesh.model_1D
- Soil parameter files (fort.15 and 18) BCsoil.table (old), vGsoil.table (new)
- Vegetation parameter file (fort.16) zvege.table_1D
- Input LAI and root profile file (fort.17) zvege.profile_1D

h) Output data: SOLVEG/OUTPUT/

- Standard output files (fort.6)	outlist
- Meteorological variable file (fort.20)	dbout
- Aerosol concentration input file (fort.21)	PMINPout
- Gas concentration input file (fort.22)	GASINPout
- Meteorological input file (fort.23)	METout
- Surface flux file (fort.24)	FLXout
- Wind speed file (fort.25)	WNDout
- Atmospheric CO2 file (fort.26)	ACO2out
- Atmospheric CO2 budget file (fort.27)	BACO2out
- Soil variable file (fort.30)	mnout
- Soil temperature file (fort.31)	TSout
- Soil water content file (fort.32)	HWout
- Soil humidity file (fort.33)	QSout
- Soil evaporation file (fort.34)	EBout
- Soil surface flux file (fort.35)	SFout
- Water retention curve (fort.36)	wcurve
- Soil thermal property (fort.37)	CSRSout
- Canopy variable file (fort.40)	VGout
- Canopy water budget file (fort.41)	VWout
- Canopy heat budget file (fort.42)	VTout
- Canopy radiation file (fort.43)	RADout
- Fog deposition and precipitation (fort.44)	PREout
- Soil CO2 file (fort.50)	SCO2out
- Canopy CO2 file (fort.51)	VCO2out
- Soil CO2 production file (fort.52)	PSCO2out
- Soil CO2 budget file (fort.53)	BSCO2out
- Aerosol concentration profile file (fort.60)	PMCout
- Aerosol flux file (fort.61)	PMFLXout
- Canopy aerosol capture file (fort.62)	VPMout
- Size-resolved aerosol deposition file (fort.160-)	VDGFoutXX(species number)
- Gas concentration profile file (fort.70)	GASCout
- Gas flux file (fort.71)	GASFLXout
- Soil ice content file (fort.81)	HIout
- Snow temperature file (fort.82)	TSNout
- Snow liquid water content file (fort.83)	HSNout
- Bulk snow density file (fort.84)	SNRout
- Snow phase change rate file (fort.85)	EMLout

- Snow ice content file (fort.86) WICEout
- Snow grain size file (fort.87) GRNout
- Vegetation growth file (fort.91, daily) VGRWout
- Vegetation biomass file (fort.92, daily) BIOMout
- Sink/source strength file (fort.93, daily) SISOout
- Active pool SOC content file (fort.101, daily) SOC1out
- Slow pool SOC content file (fort.102, daily) SOC2out
- Passive pool SOC content file (fort.103, daily) SOC3out
- SOC and DOC budget file (fort.104, daily) BSDOCout
- Active pool DOC content file (fort.105, daily) DOC1out
- Slow pool DOC content file (fort.106, daily) DOC2out
- Passive pool DOC content file (fort.107, daily) DOC3out
- Temporal output file (fort.99) tmpout

5.2. Settings and compilation of the model

Before the model users go on to compile and run the model, the prm_grid.f file in the SRC directory should be set to correct values of vertical grids for atmosphere (N1 and M1), vegetation (NC) and soil layers (NS). Note that the number of vegetation layers is smaller than that of atmosphere; i.e., NC < N1. The numbers of total horizontal grids NX (x-direction) and NY (y-direction), and the grids for output file IX and JY are set to unity because of a one-dimensional calculation. The parameter NA should be set to the layer number where atmospheric variables are generated at the OUTPUT directory. The number of gas (NGS) and aerosol species (NAS), and bin size for each aerosol species (MANP) are also given for SOLVEG run with gas and aerosol deposition. The species names and concentrations of gases and aerosols must be provided from the files of gasdata.dat (gas), fpmdata.dat (fine aerosol mode), and cpmdata.dat (coarse aerosol mode) in SOLVEG/INPUT directory. The name and parameters of available gas and aerosol species are listed in prm_gasspc.f, prm_nrspc.f, and prm_iospc.f. Tables 5-1, 5-2, 5-3, and 5-4 are examples of input data files.

With above settings, a compilation of the model begins by typing ‘make clean’ and ‘make’ at SOLVEG/SRC directory. After the execution of this script normally terminates, the execution file of SOLVEG named zsolveg_1D.exe must be created at the root directory.

It should be noted that, if the module files beginning with “prm_” are modified, the user should always require to type “make clean” and then “make” as appropriate compilation.

Table 5-1 Example of input meteorological data file (metdata.dat)

TIME	P	RS	RL	RR	U	V	T	Q	WL	CO2	SNR
2013-01-01_0000	943.00	0.00	237.00	0.00	0.69	0.45	270.60	3.01	0.00	400.00	0.00
2013-01-01_0030	943.00	0.00	236.43	0.00	-0.62	0.25	270.00	2.93	0.00	400.00	0.00
… repeat until the end time of the calculation period											

*P: surface pressure [hPa], RS: solar radiation flux [W m^{-2}], RL: long-wave radiation flux [W m^{-2}], RR: rain intensity [mm h^{-1}], U: wind u-component [m s^{-1}], V: wind v-component [m s^{-1}], T: air temperature [K], Q: specific humidity [g kg^{-1}], WL: cloud liquid water content [g m^{-3}], CO2: CO_2 concentration [ppmv], and SNR: snowfall rate [mm h^{-1}].

Table 5-2 Example of input atmospheric gas data file (gasdata.dat) with NGS ≤ 7.

TIME	O3	SO2	NO2	NH3	HNO3	NO	HCL
2013-08-01_0000	1.00	1.00	1.00	1.00	1.00	1.00	1.00
2013-08-02_1200	0.80	1.00	1.00	1.00	1.00	1.00	1.00
2013-08-02_1800	0.20	1.00	1.00	1.00	1.00	1.00	1.00
2013-08-03_0000	1.50	1.00	1.00	1.00	1.00	1.00	1.00
… repeat until the end time of the calculation period							

*The unit is ppbv for all of gas species.

Table 5-3 Example of input fine aerosol data file (fpmdata.dat) with NAS ≤ 8.

TIME	FSO4	FNO3	FNH4	FCL	FNA	FK	FMG	FCA
2013-08-01_0000	1.00	1.00	1.00	1.00	1.00	1.00	1.00	1.00
2013-08-02_1200	0.10	1.00	1.00	1.00	1.00	1.00	1.00	1.00
2013-08-04_0000	1.20	1.00	1.00	1.00	1.00	1.00	1.00	1.00
2013-08-06_1500	0.50	1.00	1.00	1.00	1.00	1.00	1.00	1.00
… repeat until the end time of the calculation period								

*The unit is μg m^{-3} for all variables.

Table 5-4 Example of input coarse aerosol data file (cpmdata.dat) with NAS ≤ 8.

TIME	CSO4	CNO3	CNH4	CCL	CNA	CK	CMG	CCA
2013-08-01_0000	1.00	1.00	1.00	1.00	1.00	1.00	1.00	1.00
2013-08-02_1600	0.50	1.00	1.00	1.00	1.00	1.00	1.00	1.00
2013-08-03_0300	0.10	1.00	1.00	1.00	1.00	1.00	1.00	1.00
2013-08-06_1200	1.50	1.00	1.00	1.00	1.00	1.00	1.00	1.00
… repeat until the end time of the calculation period								

*The unit is μg m^{-3} for all variables.

5.3. Running the model and visualization

In SRC directory, the grid number is set in prm_grid.f for your one-dimentional calculation domains.

In INPUT directory, the input file of usually hourly or half-hourly meteorological data (metdata.dat) covering throughout the calculation period is necessary for model run.

In PARAMETER directory, vertical mesh sizes should be set in the zmesh.model_1D file based on SRC/prm_grid.f. The vegetation profile file (zvege.profile_1D) also needs to be modified to specify variations in the whole calculation period by specifying vertical distributions of vegetation type (VTYPE), leaf area density (AZ), and root fraction for each vegetation type. The vegetation type is chosen from the vegetation parameter file (zvege.table_1D), which is specified by two integers: the former represents the category of vegetation, and the latter the spatial or temporal variation of them. In param_1D, the simulation condition such as calculation period, output interval is specified.

The model execution will begin by typing "./go_1D.sh" or submit as a batch job over SQL environment at the root directory. Several options of modelled processes for sensitivity tests are available in go_1D.sh:

a) iffog: Fog deposition calculation (0 = no, 1 = yes);
- npdsd: Droplet size distribution of cloud water (1-4; only work with iffog=1)

b) ifdsl: Dry soil layer (DSL) calculation (0 = no, 1 = yes)
- npwrc: Soil water retention curve (1-2; only work with ifdsl=0)
- nstms: Soil thermal conductivity (1-2; only work with ifdsl=1)

c) ifsnw: Snow/soil freeze-thaw (0 = no, 1 = yes)
- nsnfl: Snowfall input (1-2; only work with ifsnw=1)

d) ifco2: CO_2 exchange (0 = no, 1 = yes)

e) ifgas: Trace gas exchange (0 = no, 1 = yes)

f) ifpm: Particulate matter (PM) deposition (0 = no, 1 = yes)
- ifgf: Hygroscopic growth of aerosols (1 = yes, 0 = no; only work with ifpm=1)

g) ifveg: Plant growth for grassland ecosystem (0 = no, 1 = yes)

For debugging the output data, the core-dump file (core.XXXXX) is created in case there are errors in the program. The user may use debugger programs, e.g., gdb (GNU Project Debugger; https://www.gnu.org/software/gdb/) to find errors in the program. The debug run is available when "ifcore = 1" and the certain number of core-dump file is given to "ncore" in go_1D.sh.

The output files of SOLVEG can be visualized by using gnuplot software (freely available at http://gnuplot.sourceforge.net/). Sample programs for R software (freely available at https://www.r-project.org/) is also available in SOLVEG/R directory to visualize model results as shown in Fig. 5-2.

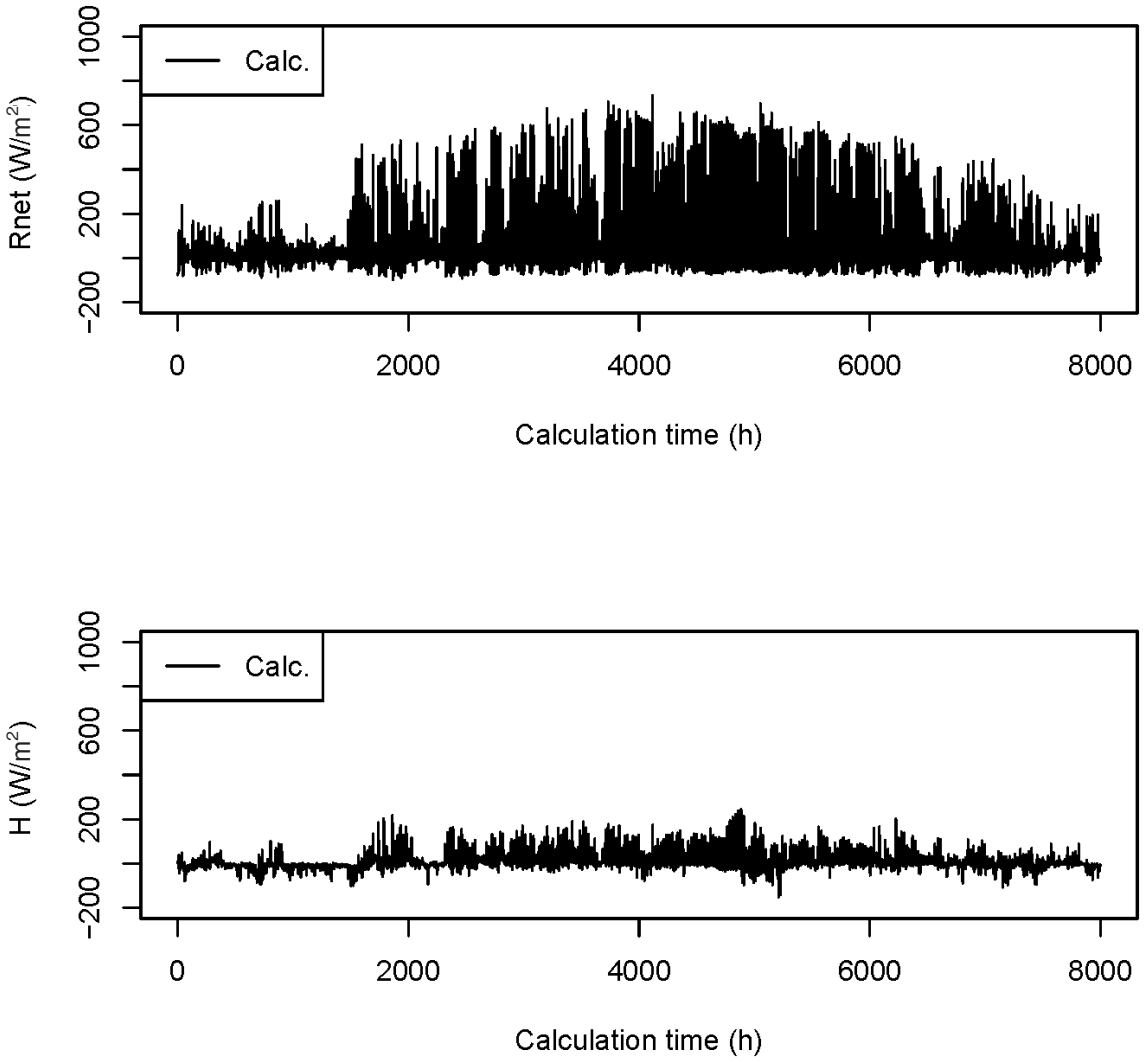

Fig. 5-2 Example output of SOLVEG calculations using a sample R shell-script. Upper and lower panels are the net radiation (Rnet) and sensible heat flux (H), respectively.

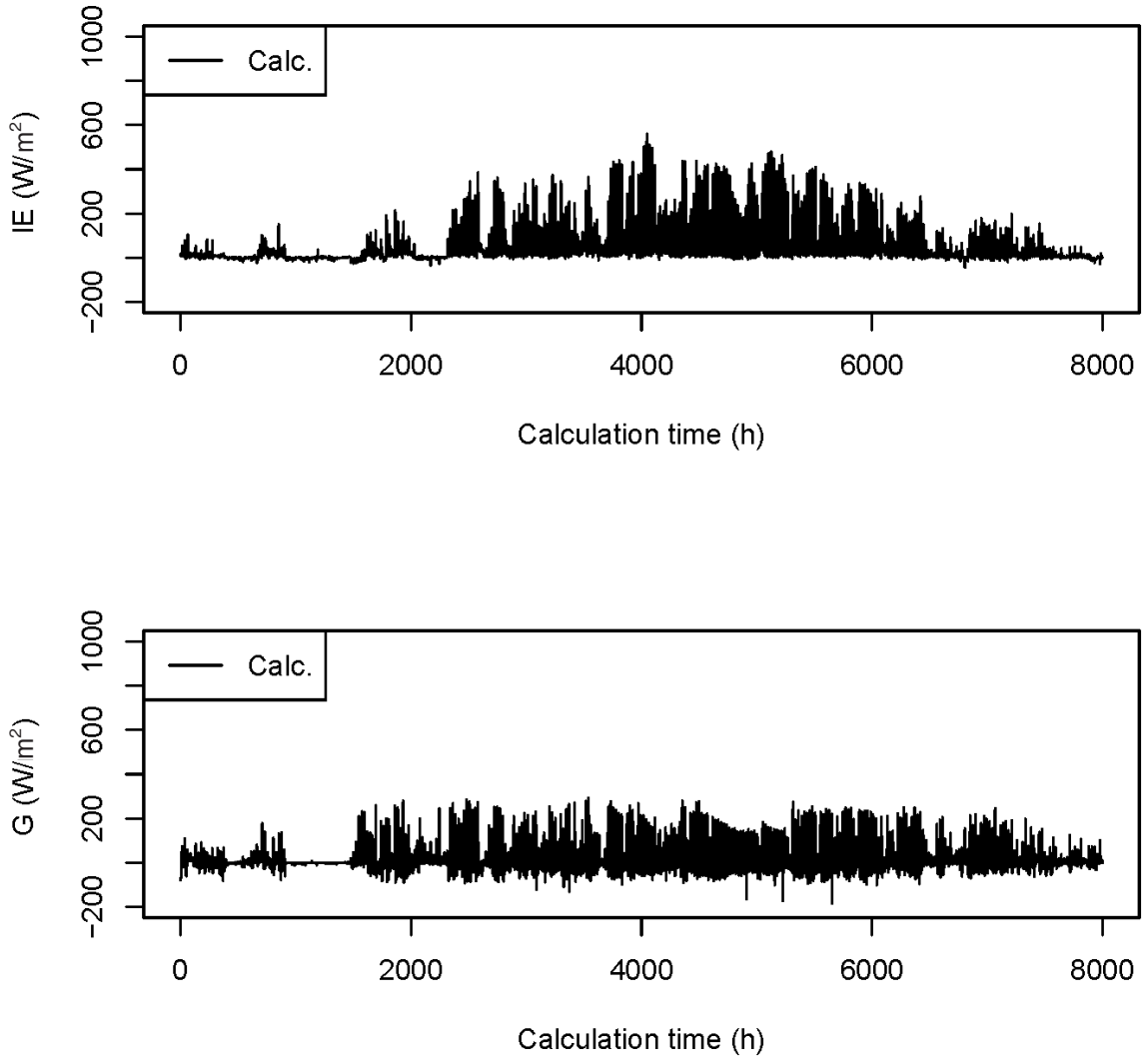

Fig. 5-2 Continued; upper and lower panels are the latent heat (lE) and soil heat flux (G), respectively.

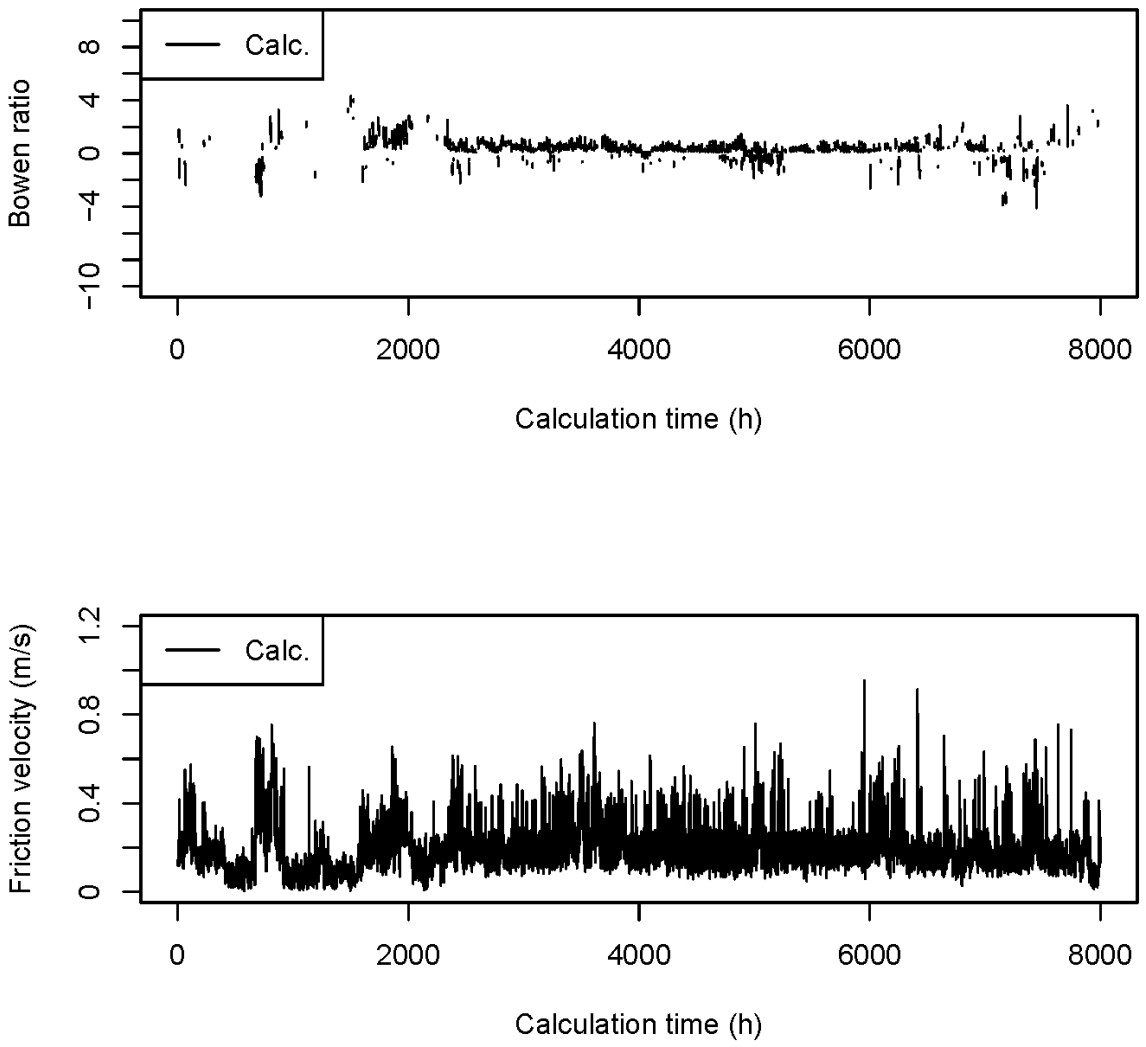

Fig. 5-2 Continued; upper and lower panels are the Bowen ratio (H/lE) and friction velocity, respectively.

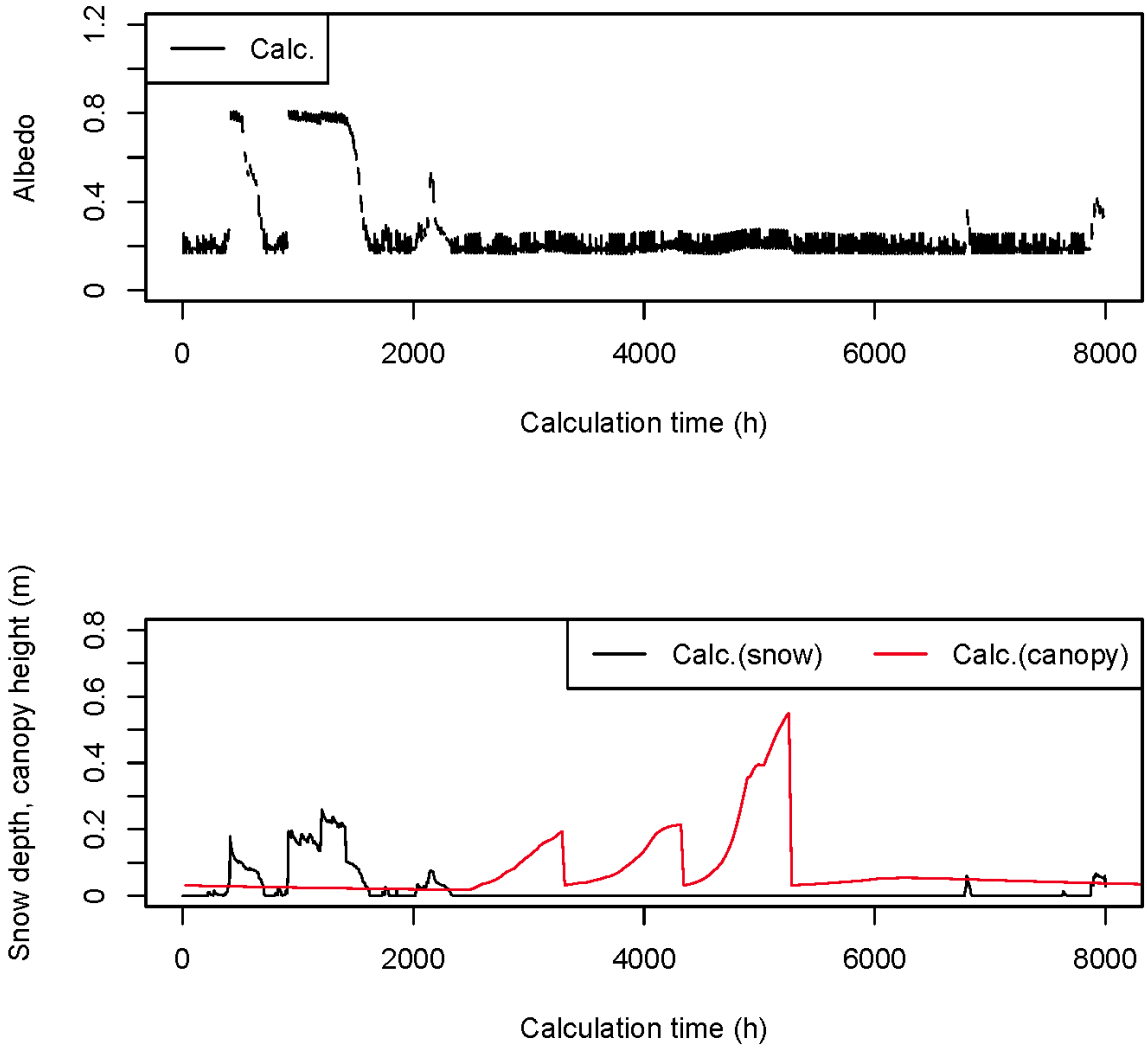

Fig. 5-2 Continued; upper and lower panels are the albedo, and snow depth and canopy height, respectively. Sudden declines in canopy height represent the grass harvest events.

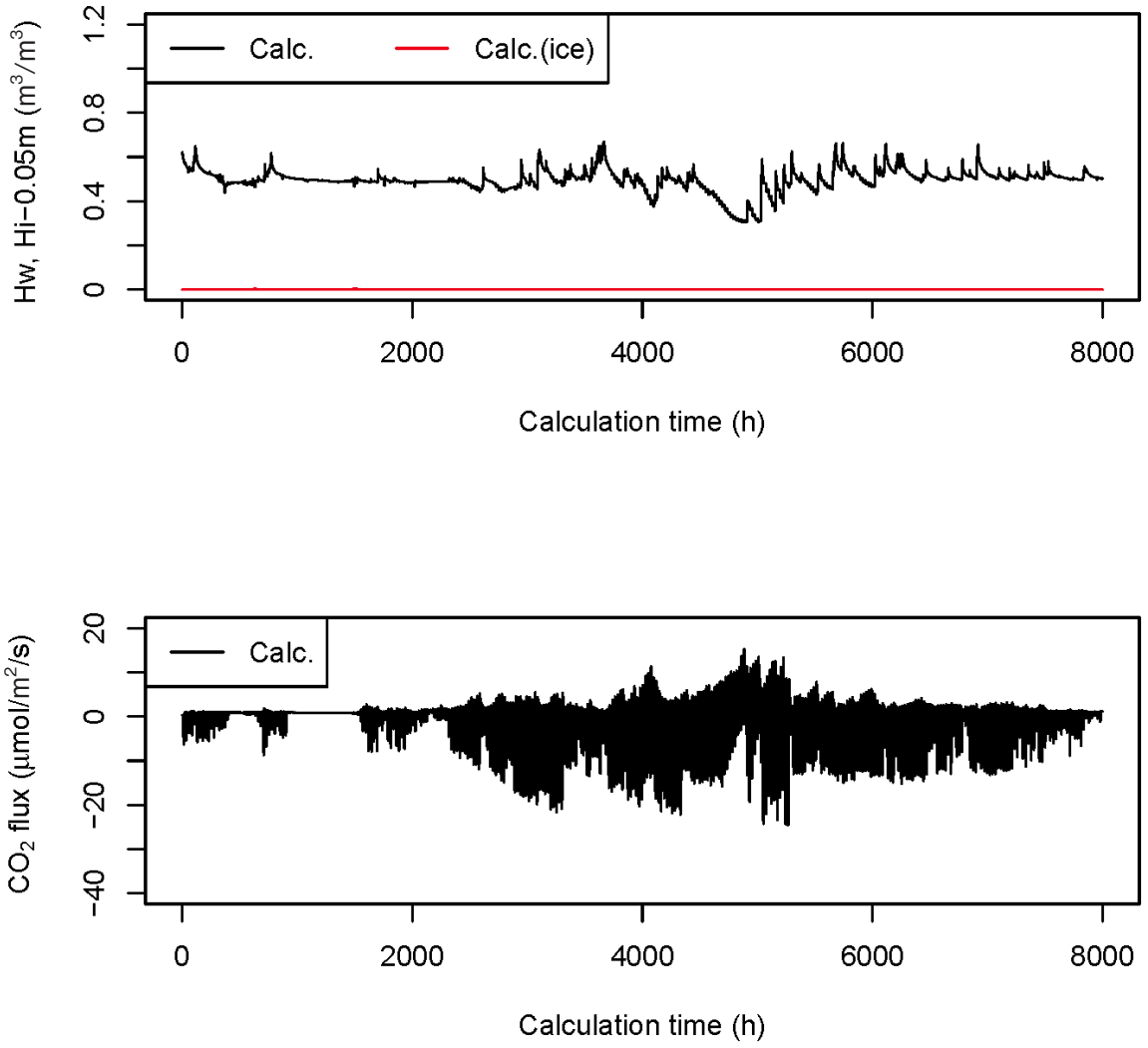

Fig. 5-2 Continued; upper and lower panels are the volumetric soil liquid water and ice content and CO_2 flux, respectively.

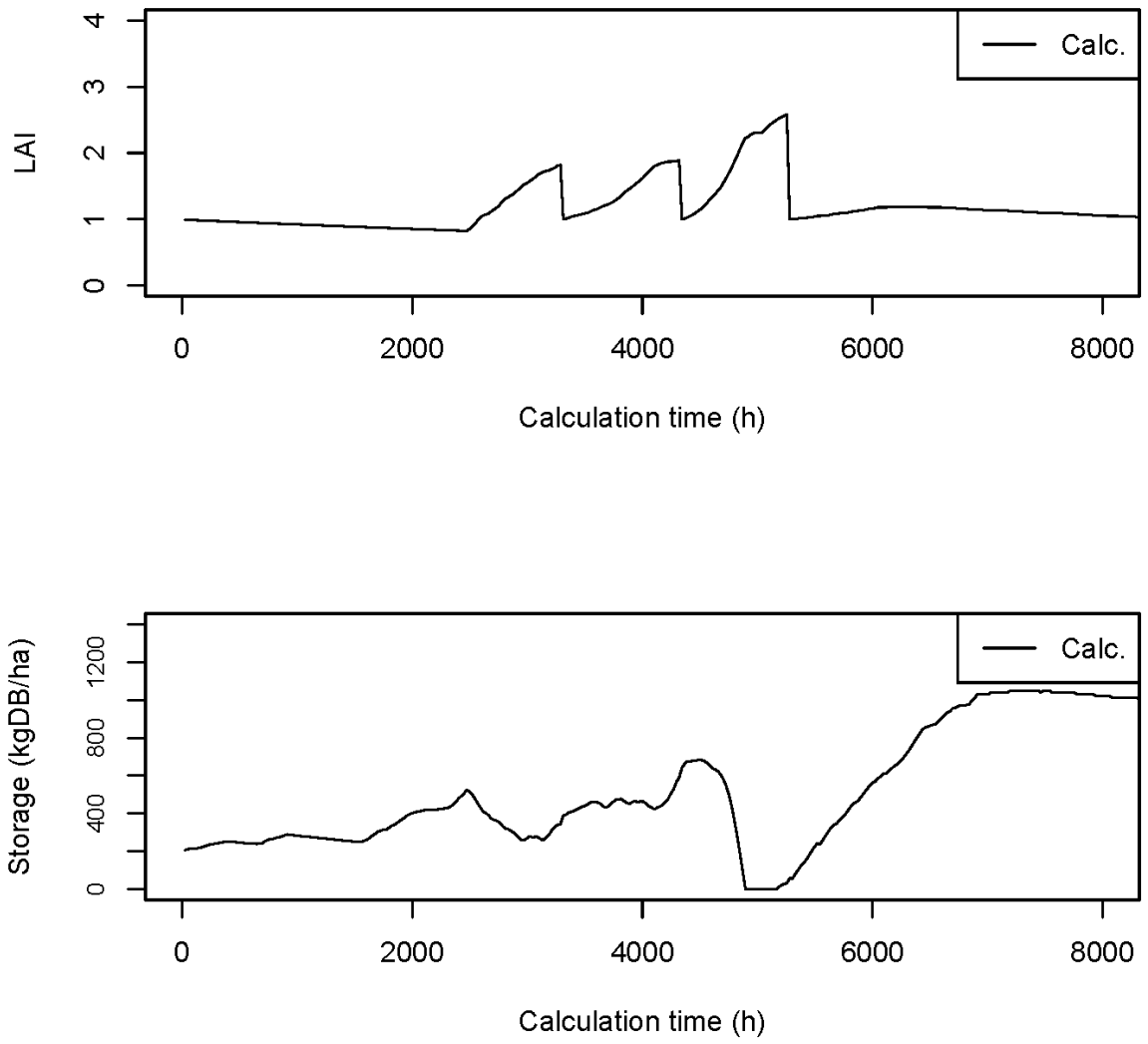

Fig. 5-2 Continued; upper and lower panels are the leaf area index (LAI) and carbohydrate storage of vegetation, respectively. Sudden declines in LAI represent the grass harvest events.

6. Summary

To investigate the impacts of atmospheric pollutants (gases and aerosols) on terrestrial ecosystems, the processes of dry deposition and emission of gases and aerosols, snow accumulation and melting, soil freeze-thaw, vegetation growth, and soil organic carbon cycle were implemented in the ecosystem model SOLVEG. The details of newly incorporated schemes were documented in this report. Further application of the model to various environmental issues will be expected to understand the complicated interaction among human activities, climate changes, and terrestrial ecosystem responses.

Acknowledgement

This study was partially supported by a Postdoctoral Fellowship for Research Abroad and a Grant-in-Aid for Scientific Research by the Japan Society for the Promotion of Science (JSPS).

References

1) H. Nagai: "Atmosphere-soil-vegetation model including CO_2 exchange processes: SOLVEG2", JAERI-Data/Code 2004-014 (2004), 92p.
2) G. Katata: "Improvement of a land surface model for accurate prediction of surface energy and water balances", JAEA-Data/Code 2008-033 (2009), 64p.
3) G. Katata, H, Nagai, H. Ueda, N. Agam, P.R. Berliner: "Development of a Land Surface Model Including Evaporation and Adsorption Processes in the Soil for the Land–Air Exchange in Arid Regions", Journal of Hydrometeorology, 8, pp. 1307-1324 (2007).
4) H. Nagai: "Validation and sensitivity analysis of a new atmosphere-soil-vegetation model", Journal of Applied Meteorology, 41, pp. 160-176 (2002).
5) H. Nagai: "Validation and sensitivity analysis of a new atmosphere-soil-vegetation model. Part II: Impacts on in-canopy latent heat flux over a winter wheat field determined by detailed calculation of canopy radiation transmission and stomatal resistance", Journal of Applied Meteorology, 42, pp. 434-451 (2003).
6) G. Katata, K. Hayashi, K. Ono, H. Nagai, A. Miyata, M. Mano: "Coupling atmospheric ammonia exchange process over a rice paddy field with a multi-layer atmosphere-soil-vegetation model", Agricultural and Forest Meteorology, 180, pp. 1-21 (2013).
7) H. Nagai: "Incorporation of CO_2 exchange processes into a multilayer atmosphere-soil-vegetation model", Journal of Applied Meteorology, 44, pp. 1574-1592 (2005).
8) M. Ota, H. Nagai, J. Koarashi: "Root and dissolved organic carbon controls on subsurface soil carbon dynamics: A model approach", Journal of Geophysical Research, 118, pp. 1646-1659 (2013).
9) G. Katata, H. Nagai, T. Wrzesinsky, O. Klemm, W. Eugster, R. Burkard: "Development of a Land Surface Model Including Cloud Water Deposition on Vegetation", Journal of Applied Meteorology and Climatology, 47, pp. 2129-2146 (2008).
10) G. Katata, H. Nagai, L. Zhang, A. Held, D. Serça, O. Klemm: "Development of an atmosphere-soil-vegetation model for investigation of radioactive materials transport in the terrestrial biosphere", Progress in Nuclear Science and Technology, 2, pp. 530-537 (2011).
11) G. Katata, M. Kajino, K. Matsuda, A. Takahashi, K. Nakaya: "A numerical study of the effects of aerosol hygroscopic properties to dry deposition on a broad-leaved forest", Atmospheric Environment, 97, pp. 501-510 (2014).
12) A.R. Desai, M. Wohlfahrt, M.J. Zeeman, G. Katata, W. Eugster, L. Montagnani, D. Gianelle, M. Mauder, H-P. Schmid: "Montane ecosystem productivity responds more to global circulation patterns than climatic trends", Environmental Research Letters, 11,

p. 024013 (2016).

13) B.J. Huebert, C.H. Robert: "The dry deposition of nitric-acid to grass", Journal of Geophysical Research, 90, pp. 2085-2090 (1985).

14) L. Zhang, L.P. Wright, W.A.H. Asman: "Bi-directional air-surface exchange of atmospheric ammonia: A review of measurements and a development of a big-leaf model for applications in regional-scale air-quality models", Journal of Geophysical Research, 115, pp. D20310 (2010).

15) L.W.A. Van Hove, E.H. Adema, W.J. Vredenberg: “A study of the adsorption of NH_3 and SO_2 on leaf surfaces”, Atmospheric Environment, 23, pp. 1479-1486 (1989).

16) L. Zhang, S. Gong, J. Padro, L. Barrie: "A size-segregated particle dry deposition scheme for an atmospheric aerosol module", Atmospheric Environment, 35, pp. 549-560 (2001).

17) M.D. Petters, S.M. Kreidenweis: "A single parameter representation of hygroscopic growth and cloud condensation nucleus activity", Atmospheric Chemistry and Physics, 7, pp. 1961-1971 (2007).

18) N.A. Fuchs, A.G. Sutugin: "Highly dispersed aerosols. Hidy G.M., Brock J.R. (Eds). Topics in Current Aerosol Research, vol. 2. Pergamon”, New York, pp. 1-60 (1971).

19) C. Fountoukis, A. Nenes: "ISORROPIA II: a computationally efficient thermodynamic equilibrium model for K^+-Ca^{2+}-Mg^{2+}-NH^+-Na^+-SO_4^{2-}-NO_3^--Cl^--H_2O aerosols", Atmospheric Chemistry and Physics, 7, pp. 4639-4659 (2007).

20) K.W. Oleson, D.M. Lawrence, G.B. Bonan, M.G. Flanner, E. Kluzek, P.J. Lawrence, S. Levis, S.C. Swenson, P.E. Thornton: "Technical description of version 4.0 of the Community Land Model (CLM)", NCAR Technical Note NCAR/TN-461+STR, National Center for Atmospheric Research, Boulder, CO (2010).

21) R. Jordan: "A one-dimensional temperature model for a snow cover", Technical documentation for SNTHERM.89, CRREL Special Report 91-16, US Army Core of Engineers Cold Regions Research and Engineering Laboratory, Hanover, NH (1991).

22) H. Hirashima, S. Yamaguchi, A. Sati, M. Lehning: "Numerical modeling of liquid water movement through layered snow based on new measurements of the water retention curve", Cold Regions Science and Technology, 64, pp. 94-103 (2010).

23) T. Yamazaki: "A one-dimensional land surface model adaptable to intensely cold regions and its applications in eastern siberia", Journal of the Meteorological Society of Japan, 79, pp. 1107-1118 (2001).

24) W.J. Wiscombe, SG Warren: "A model for the spectral albedo of snow. I: pure snow", Journal of Atmospheric Science, 37, pp. 2712-2733 (1980).

25) R. Essery, S. Morin, Y. Lejeune, C.B. Ménard: "A comparison of 1701 snow models using observations from an alpine site", Advances in Water Resources, 55, pp. 131-148 (2013).

26) A. Boone: "Description du schema de neige ISBA-ES (Explicit Snow)", Centre National

de Recherches Météorologiques, Météo-France, Toulouse (2002). Available from: http://www.cnrm.meteo.fr/IMG/pdf/snowdoc.pdf (accessed on December 5, 2016)

27) X. Zhang, S. Sun, Y. Xue: "Development and testing of a frozen soil parameterization for cold region studies", Journal of Hydrometeorology, vol. 8, issue 4, pp. 690-701 (2007).

28) A.H.M.C. Schapendonk, W. Stol, D.W.G. van Kraalingen, B.A.M. Bouman: "LINGRA – a source/sink model to simulate grassland productivity in Europe", European Journal of Agronomy, 9, pp. 87-100 (1998).

29) M. Höglind, A.H.C.M. Schapendonk, M. van Oijene: "Timothy growth in Scandinavia: combining quantitative information and simulation modelling", New Phytologist, 151, pp. 355-367 (2001).

30) A. Mäkelä, P. Hari, F. Berninger, H. Hänninen, E. Nikinmaa: "Acclimation of photosynthetic capacity in Scots pine to the annual cycle of temperature", Tree Physiology, 24, pp. 369-376 (2004).

31) V. Arora, G.J. Boer: "A parameterization of leaf phenology for the terrestrial ecosystem component of climate models", Global Change Biology, 11, pp. 39-59 (2005).

32) V. Arora, G.J. Boer: "A representation of variable root distribution in dynamic vegetation models", Earth Interactions, 7, pp. 1-19 (2003).

This is a blank page.

国際単位系（SI）

表１．SI 基本単位

基本量	SI 基本単位	
	名称	記号
長さ	メートル	m
質量	キログラム	kg
時間	秒	s
電流	アンペア	A
熱力学温度	ケルビン	K
物質量	モル	mol
光度	カンデラ	cd

表２．基本単位を用いて表されるSI組立単位の例

組立量	SI 組立単位	
	名称	記号
面積	平方メートル	m^2
体積	立方メートル	m^3
速さ，速度	メートル毎秒	m/s
加速度	メートル毎秒毎秒	m/s^2
波数	毎メートル	m^{-1}
密度，質量密度	キログラム毎立方メートル	kg/m^3
面積密度	キログラム毎平方メートル	kg/m^2
比体積	立方メートル毎キログラム	m^3/kg
電流密度	アンペア毎平方メートル	A/m^2
磁界の強さ	アンペア毎メートル	A/m
量濃度(a)，濃度	モル毎立方メートル	mol/m^3
質量濃度	キログラム毎立方メートル	kg/m^3
輝度	カンデラ毎平方メートル	cd/m^2
屈折率(b)	（数字の） 1	1
比透磁率(b)	（数字の） 1	1

(a) 量濃度（amount concentration）は臨床化学の分野では物質濃度（substance concentration）ともよばれる。
(b) これらは無次元量あるいは次元１をもつ量であるが、そのことを表す単位記号である数字の１は通常は表記しない。

表３．固有の名称と記号で表されるSI組立単位

組立量	SI 組立単位			
	名称	記号	他のSI単位による表し方	SI基本単位による表し方
平面角	ラジアン(b)	rad	1 (b)	m/m
立体角	ステラジアン(b)	sr(c)	1 (b)	m^2/m^2
周波数	ヘルツ(d)	Hz		s^{-1}
力	ニュートン	N		$m\ kg\ s^{-2}$
圧力，応力	パスカル	Pa	N/m^2	$m^{-1}\ kg\ s^{-2}$
エネルギー，仕事，熱量	ジュール	J	N m	$m^2\ kg\ s^{-2}$
仕事率，工率，放射束	ワット	W	J/s	$m^2\ kg\ s^{-3}$
電荷，電気量	クーロン	C		s A
電位差（電圧），起電力	ボルト	V	W/A	$m^2\ kg\ s^{-3}\ A^{-1}$
静電容量	ファラド	F	C/V	$m^{-2}\ kg^{-1}\ s^4\ A^2$
電気抵抗	オーム	Ω	V/A	$m^2\ kg\ s^{-3}\ A^{-2}$
コンダクタンス	ジーメンス	S	A/V	$m^{-2}\ kg^{-1}\ s^3\ A^2$
磁束	ウエーバ	Wb	Vs	$m^2\ kg\ s^{-2}\ A^{-1}$
磁束密度	テスラ	T	Wb/m^2	$kg\ s^{-2}\ A^{-1}$
インダクタンス	ヘンリー	H	Wb/A	$m^2\ kg\ s^{-2}\ A^{-2}$
セルシウス温度	セルシウス度(e)	℃		K
光束	ルーメン	lm	cd sr(c)	cd
照度	ルクス	lx	lm/m^2	m^{-2} cd
放射性核種の放射能(f)	ベクレル(d)	Bq		s^{-1}
吸収線量，比エネルギー分与，カーマ	グレイ	Gy	J/kg	$m^2\ s^{-2}$
線量当量，周辺線量当量，方向性線量当量，個人線量当量	シーベルト(g)	Sv	J/kg	$m^2\ s^{-2}$
酸素活性	カタール	kat		s^{-1} mol

(a)SI接頭語は固有の名称と記号を持つ組立単位と組み合わせても使用できる。しかし接頭語を付した単位はもはやコヒーレントではない。
(b)ラジアンとステラジアンは数字の１に対する単位の特別な名称で、量についての情報をつたえるために使われる。実際には、使用する時には記号radおよびsrが用いられるが、習慣として組立単位としての記号である数字の１は明示されない。
(c)測光学ではステラジアンという名称と記号srを単位の表し方の中に、そのまま維持している。
(d)ヘルツは周期現象についてのみ、ベクレルは放射性核種の統計的過程についてのみ使用される。
(e)セルシウス度はケルビンの特別な名称で、セルシウス温度を表すために使用される。セルシウス度とケルビンの単位の大きさは同一である。したがって、温度差や温度間隔を表す数値はどちらの単位で表しても同じである。
(f)放射性核種の放射能（activity referred to a radionuclide）は、しばしば誤った用語で"radioactivity"と記される。
(g)単位シーベルト（PV,2002,70,205）についてはCIPM勧告2（CI-2002）を参照。

表４．単位の中に固有の名称と記号を含むSI組立単位の例

組立量	SI 組立単位		
	名称	記号	SI 基本単位による表し方
粘度	パスカル秒	Pa s	$m^{-1}\ kg\ s^{-1}$
力のモーメント	ニュートンメートル	N m	$m^2\ kg\ s^{-2}$
表面張力	ニュートン毎メートル	N/m	$kg\ s^{-2}$
角速度	ラジアン毎秒	rad/s	$m\ m^{-1}\ s^{-1}=s^{-1}$
角加速度	ラジアン毎秒毎秒	rad/s^2	$m\ m^{-1}\ s^{-2}=s^{-2}$
熱流密度，放射照度	ワット毎平方メートル	W/m^2	$kg\ s^{-3}$
熱容量，エントロピー	ジュール毎ケルビン	J/K	$m^2\ kg\ s^{-2}\ K^{-1}$
比熱容量，比エントロピー	ジュール毎キログラム毎ケルビン	J/(kg K)	$m^2\ s^{-2}\ K^{-1}$
比エネルギー	ジュール毎キログラム	J/kg	$m^2\ s^{-2}$
熱伝導率	ワット毎メートル毎ケルビン	W/(m K)	$m\ kg\ s^{-3}\ K^{-1}$
体積エネルギー	ジュール毎立方メートル	J/m^3	$m^{-1}\ kg\ s^{-2}$
電界の強さ	ボルト毎メートル	V/m	$m\ kg\ s^{-3}\ A^{-1}$
電荷密度	クーロン毎立方メートル	C/m^3	m^{-3} s A
表面電荷	クーロン毎平方メートル	C/m^2	m^{-2} s A
電束密度，電気変位	クーロン毎平方メートル	C/m^2	m^{-2} s A
誘電率	ファラド毎メートル	F/m	$m^{-3}\ kg^{-1}\ s^4\ A^2$
透磁率	ヘンリー毎メートル	H/m	$m\ kg\ s^{-2}\ A^{-2}$
モルエネルギー	ジュール毎モル	J/mol	$m^2\ kg\ s^{-2}\ mol^{-1}$
モルエントロピー，モル熱容量	ジュール毎モル毎ケルビン	J/(mol K)	$m^2\ kg\ s^{-2}\ K^{-1}\ mol^{-1}$
照射線量（X線及びγ線）	クーロン毎キログラム	C/kg	kg^{-1} s A
吸収線量率	グレイ毎秒	Gy/s	$m^2\ s^{-3}$
放射強度	ワット毎ステラジアン	W/sr	$m^4\ m^{-2}\ kg\ s^{-3}=m^2\ kg\ s^{-3}$
放射輝度	ワット毎平方メートル毎ステラジアン	$W/(m^2\ sr)$	$m^2\ m^{-2}\ kg\ s^{-3}=kg\ s^{-3}$
酵素活性濃度	カタール毎立方メートル	kat/m^3	$m^{-3}\ s^{-1}$ mol

表５．SI 接頭語

乗数	名称	記号	乗数	名称	記号
10^{24}	ヨタ	Y	10^{-1}	デシ	d
10^{21}	ゼタ	Z	10^{-2}	センチ	c
10^{18}	エクサ	E	10^{-3}	ミリ	m
10^{15}	ペタ	P	10^{-6}	マイクロ	μ
10^{12}	テラ	T	10^{-9}	ナノ	n
10^9	ギガ	G	10^{-12}	ピコ	p
10^6	メガ	M	10^{-15}	フェムト	f
10^3	キロ	k	10^{-18}	アト	a
10^2	ヘクト	h	10^{-21}	ゼプト	z
10^1	デカ	da	10^{-24}	ヨクト	y

表６．SIに属さないが、SIと併用される単位

名称	記号	SI 単位による値
分	min	1 min=60 s
時	h	1 h =60 min=3600 s
日	d	1 d=24 h=86 400 s
度	°	1°=(π/180) rad
分	’	1’=(1/60)°=(π/10 800) rad
秒	”	1”=(1/60)’=(π/648 000) rad
ヘクタール	ha	1 ha=1 $hm^2=10^4m^2$
リットル	L, l	1 L=1 l=1 $dm^3=10^3cm^3=10^{-3}m^3$
トン	t	1 t=10^3 kg

表７．SIに属さないが、SIと併用される単位で、SI単位で表される数値が実験的に得られるもの

名称	記号	SI 単位で表される数値
電子ボルト	eV	1 eV=1.602 176 53(14)×10^{-19}J
ダルトン	Da	1 Da=1.660 538 86(28)×10^{-27}kg
統一原子質量単位	u	1 u=1 Da
天文単位	ua	1 ua=1.495 978 706 91(6)×10^{11}m

表８．SIに属さないが、SIと併用されるその他の単位

名称	記号	SI 単位で表される数値
バール	bar	1 bar=0.1MPa=100 kPa=10^5Pa
水銀柱ミリメートル	mmHg	1 mmHg≈133.322Pa
オングストローム	Å	1 Å=0.1nm=100pm=10^{-10}m
海里	M	1 M=1852m
バーン	b	1 b=100fm^2=$(10^{-12}cm)^2$=$10^{-28}m^2$
ノット	kn	1 kn=(1852/3600)m/s
ネーパ	Np	SI単位との数値的な関係は、対数量の定義に依存。
ベル	B	
デシベル	dB	

表９．固有の名称をもつCGS組立単位

名称	記号	SI 単位で表される数値
エルグ	erg	1 erg=10^{-7} J
ダイン	dyn	1 dyn=10^{-5}N
ポアズ	P	1 P=1 dyn s cm^{-2}=0.1Pa s
ストークス	St	1 St =1$cm^2\ s^{-1}$=$10^{-4}m^2\ s^{-1}$
スチルブ	sb	1 sb =1cd cm^{-2}=10^4cd m^{-2}
フォト	ph	1 ph=1cd sr cm^{-2} =10^4lx
ガル	Gal	1 Gal =1cm s^{-2}=$10^{-2}ms^{-2}$
マクスウエル	Mx	1 Mx = 1G cm^2=10^{-8}Wb
ガウス	G	1 G =1Mx cm^{-2} =10^{-4}T
エルステッド(a)	Oe	1 Oe ≙ $(10^3/4\pi)$A m^{-1}

(a) ３元系のCGS単位系とSIでは直接比較できないため、等号「 ≙ 」は対応関係を示すものである。

表10．SIに属さないその他の単位の例

名称	記号	SI 単位で表される数値
キュリー	Ci	1 Ci=3.7×10^{10}Bq
レントゲン	R	1 R = 2.58×10^{-4}C/kg
ラド	rad	1 rad=1cGy=10^{-2}Gy
レム	rem	1 rem=1 cSv=10^{-2}Sv
ガンマ	γ	1 γ=1 nT=10^{-9}T
フェルミ		1 フェルミ=1 fm=10^{-15}m
メートル系カラット		1 メートル系カラット= 0.2 g = 2×10^{-4}kg
トル	Torr	1 Torr = (101 325/760) Pa
標準大気圧	atm	1 atm = 101 325 Pa
カロリー	cal	1 cal=4.1858J（「15℃」カロリー），4.1868J（「IT」カロリー），4.184J（「熱化学」カロリー）
ミクロン	μ	1 μ =1μm=10^{-6}m

（第8版，2006年）